Non-Abelian Kuramoto models and synchronization

2009 J. Phys. A: Math. Theor. 42 395101

(http://iopscience.iop.org/1751-8121/42/39/395101)

IOP PUBLISHING JOURNAL OF PHYSICS A: MATHEMATICAL AND THEORETICAL

J. Phys. A: Math. Theor. **42** (2009) 395101 (25pp) doi:10.1088/1751-8113/42/39/395101

Non-Abelian Kuramoto models and synchronization

M A Lohe

Department of Physics, The University of Adelaide, 5005, Australia

E-mail: Max.Lohe@adelaide.edu.au

Received 1 June 2009, in final form 24 July 2009
Published 11 September 2009
Online at stacks.iop.org/JPhysA/42/395101

Abstract

We describe non-Abelian generalizations of the Kuramoto model for any classical compact Lie group and identify their main properties. These models may be defined on any complex network where the variable at each node is an element of the unitary group $U(n)$, or a subgroup of $U(n)$. The nonlinear evolution equations maintain the unitarity of all variables which therefore evolve on the compact manifold of $U(n)$. Synchronization of trajectories with phase locking occurs as for the Kuramoto model, for values of the coupling constant larger than a critical value, and may be measured by various order and disorder parameters. Limit cycles are characterized by a frequency matrix which is independent of the node and is determined by minimizing a function which is quadratic in the variables. We perform numerical computations for $n = 2$, for which the $SU(2)$ group manifold is S^3, for a range of natural frequencies and all-to-all coupling, in order to confirm synchronization properties. We also describe a second generalization of the Kuramoto model which is formulated in terms of real m-vectors confined to the $(m-1)$-sphere for any positive integer m, and investigate trajectories numerically for the S^2 model. This model displays a variety of synchronization phenomena in which trajectories generally synchronize spatially but are not necessarily phase-locked, even for large values of the coupling constant.

PACS numbers: 05.45.Xt, 89.75.Fb

(Some figures in this article are in colour only in the electronic version)

1. Introduction

The phenomenon of self-synchronization in complex systems has been widely investigated, see the general accounts [1, 2], also textbooks such as [3, 4], and the review articles [5–9]. Synchronization of dynamical systems involves two or more interacting elements of a complex system, with properties that are correlated in time leading to the evolution of the system as a

collective entity, see for example the discussion in [9]. Many types of synchronization have been identified particularly for chaotic systems [6], but here we consider phase synchronization in which phases are closely or exactly correlated, and spatial synchronization in which the trajectories of connected systems are also correlated.

The first modern investigations of phase synchronized systems have been attributed to Winfree [10, 11] who studied the nonlinear dynamics of a large population of weakly coupled limit cycle oscillators, in which he assumed that the oscillators' natural frequencies were distributed about some mean value according to a prescribed probability distribution. As emphasized also in [9], amplitude variations are neglected in the limit of weak coupling and the oscillators are described solely by their phases along their limit cycles.

The Kuramoto model, proposed in 1975 [12], has been extensively investigated as a model of phase synchronization over a complex network. Its popularity has been attributed [7] to its mathematical tractability together with a level of complexity that enables the model to display a wide variety of synchronization behaviours. The Kuramoto model describes a system of weakly coupled, nearly identical interacting limit cycle oscillators where each oscillator influences the phase of oscillators to which it is connected. As is well known [5, 7, 9], when the coupling is very weak each element oscillates independently according to its natural frequency, but at an increased coupling strength partial synchronization takes place in which clusters of synchronized nodes appear, while at a sufficiently large coupling strength the system synchronizes completely to a mean frequency. For a system of N nodes the Kuramoto equations are usually written as

$$\dot{\theta}_i = \nu_i + \frac{\kappa}{N}\sum_{j=1}^{N} a_{ij}\sin(\theta_j - \theta_i), \qquad (i = 1, \ldots, N), \tag{1}$$

where θ_i is the phase angle at the ith node, $\kappa \geqslant 0$ is a coupling constant and ν_i is the natural frequency of θ_i, distributed according to a given probability distribution. The $N \times N$ matrix (a_{ij}) is the connectivity matrix where we can choose $a_{ij} = 1$ if the distinct nodes i, j are connected, and zero otherwise, but in any case the elements depend only on i, j. We refer to the reviews [5, 7, 9] for further references and for analyses of the Kuramoto model and its extensions, including discussions of fundamental topics such as the stability of solutions, the inclusion of forcing terms and various applications.

Here we describe a hierarchy of models which we term non-Abelian Kuramoto models, since the fundamental variable at each node is an $n \times n$ unitary matrix U_i corresponding to an element of the compact non-Abelian unitary group $U(n)$, or a subgroup of $U(n)$. The equations for the Abelian case $n = 1$ reduce to the simplest Kuramoto model (1) by parametrizing $U_i = \mathrm{e}^{-\mathrm{i}\theta_i}$ although we also find it convenient to parametrize each U_i according to $U_i = x_i^1 - \mathrm{i}x_i^2$ where the 2-vector $\boldsymbol{x}_i = (x_i^1, x_i^2)$ lies on the unit circle. We determine basic properties of the non-Abelian models, in particular, the existence of periodic limit cycles characterized by synchronized frequencies independent of the node i and show numerically that for sufficiently large couplings, solutions with random initial conditions synchronize to these limit cycles. We distinguish here between spatial synchronization, which refers to trajectories which are closely correlated in coordinate space and is measured by an order parameter which generalizes that defined by Kuramoto [13, p 71], and phase synchronization in which phases are either closely or exactly correlated. In the latter case 'exact' means that trajectories are numerically indistinguishable from periodic limit cycles with a common frequency, to which we refer as 'phase-locked' trajectories, and which can be measured by one or more disorder parameters as discussed also in [14].

We also describe a second generalization of the Abelian model (1) which depends on an integer m and reduces to (1) for $m = 2$, but for $m = 4$ coincides with the non-Abelian model

for $n = 2$, for which trajectories lie on the group manifold of $SU(2)$, namely the 3-sphere S^3. The trajectories in these models are described by a real m-vector x_i, which we regard as the location of a particle of unit mass, and lie in the common vector space S^{m-1}. Phase locking for general m, however, does not necessarily follow as for $m = 2$ or $m = 4$, as we demonstrate for $m = 3$. In this case, spatial synchronization occurs in the sense that trajectories on S^2 are coordinated in space, i.e. the particles bunch together in a tight spatial cluster with the unit centre-of-mass vector executing almost periodic motion on S^2, but with relative motion within the cluster so that phase synchronization takes place only in a time-averaged sense.

Both generalizations possess the feature that the relevant variables, whether the group elements U_i or the m-vectors x_i at each node, have constant amplitude or constant length as a consequence of the equations of motion, i.e. the amplitudes at every node are constants of the motion. We restrict our numerical investigations to all-to-all coupling ($a_{ij} = 1$ for all $i \neq j$) and to $N \leqslant 100$, however other work confirms our numerical findings for large values of N, and also for network couplings other than all-to-all couplings.

We firstly describe chirally covariant non-Abelian models in section 2, where the variable at each node is an $n \times n$ unitary matrix U_i, or an element of a subgroup of $U(n)$, and discuss in particular why trajectories are confined to the compact group manifold. Then in section 3 we investigate limit cycles and their properties, although our aim is not to prove stability of these limit cycles, but to identify their main properties such as the common frequency of synchronized trajectories, and how spatial and phase correlations may be measured. In section 4, we consider specifically the $SU(2)$ model, for which trajectories lie on S^3, and its generalization to an S^{m-1} model for any positive integer m. In section 5, we consider specifically the S^2 model and discuss numerical results, followed in section 6 by the S^3 model, which resembles the Abelian Kuramoto model in that trajectories are both spatially synchronized and phase-locked for sufficiently large values of the coupling constant κ, i.e. the N particles move in a synchronized phase-locked cluster on S^3. In section 7, we investigate several qualitative features of the S^{m-1} models including spatial synchronization as well as properties of the fixed point solutions and deduce, as one outcome, that synchronization can only occur for values of κ larger then a critical value κ_c. The synchronized frequency is determined by minimizing a quadratic form in the fixed points with respect to the frequency matrix.

2. Non-Abelian generalization

Recalling the identification $U_i = e^{-i\theta_i}$ for the Abelian Kuramoto model, we generalize the N equations (1) to

$$i\dot{U}_i U_i^\dagger = H_i - \frac{i\kappa}{2N}\sum_{j=1}^{N} a_{ij}\big(U_i U_j^\dagger - U_j U_i^\dagger\big), \qquad (i = 1, \ldots, N), \tag{2}$$

where the variable U_i is a complex $n \times n$ matrix, $U_i^\dagger$ denotes the Hermitean conjugate of U_i and H_i is a given $n \times n$ Hermitean matrix which therefore has real eigenvalues, which constitute the natural frequencies of the oscillator at the node i. These natural frequencies depend on the node and may be allocated random values according to a given probability distribution. The matrices H_i could also have a given time dependence but we assume here that each H_i is time independent. The connectivity matrix (a_{ij}) and the coupling constant κ, which has the dimension of inverse time, have the same meaning as before.

In (2) the variable U_i at each node i is an element of a linear vector space V_i, a subspace of $\mathbb{C}^{n^2}$. The effect of the coupling through the connectivity matrix (a_{ij}) is that a trajectory in

V_i is copied to a common vector space V, and so we regard each variable also as an element of V, where we use the same notation U_i for the variable as an element in V_i and its copy in V. Furthermore, we also regard the matrices H_i in V_i as being copied to V, and hence neither H_i nor U_i, considered as elements of V, commute for different i, and so the order of the variables U_i in the defining equations (2) must be as specified. For the Abelian Kuramoto model the common vector space V is the unit circle S^1 and the 1×1 matrices H_i, U_i commute for all i. We may plot, as is usual [5], the trajectories of all N unit 2-vectors $\boldsymbol{x}_i$ on a common unit circle.

Since H_i is Hermitean by choice and the remaining terms on the right-hand side of (2) are also Hermitean by construction, it follows that $\mathrm{i}\,\dot{U}_i U_i^\dagger = -\mathrm{i}\,U_i \dot{U}_i^\dagger$ and hence

$$\frac{\mathrm{d}}{\mathrm{d}t}\left(U_i U_i^\dagger\right) = 0. \tag{3}$$

Therefore $U_i U_i^\dagger$ is a constant of the motion at each node and so is equal to its value at the initial time $t = 0$. This implies that the amplitude of U_i is constant, where the amplitude A of any complex matrix Z is defined according to the left polar decomposition $Z = AU$, where U is unitary and A is a positive-semidefinite Hermitean matrix, with $A^2 = ZZ^\dagger$. For properties of matrix polar decompositions see for example [15], section 3.1. Although one could consider models in which this constant matrix amplitude varies according to the node, we assume here that the initial value of $U_i U_i^\dagger$ is chosen for all i to be the identity matrix I_n, and then U_i is unitary for each i for all subsequent times. For $n = 1$ we regain the Abelian Kuramoto model upon parametrizing $U_i = \mathrm{e}^{-\mathrm{i}\theta_i}$ and identifying $H_i = \nu_i$. Our formulation differs slightly from that of Kuramoto [12] which is also expressed in terms of a complex variable, in that here the constancy of the amplitude is a consequence of the equations of motion.

The fact that unitarity of U_i follows from (2) is not surprising in the uncoupled case $\kappa = 0$, for then these equations reduce at each node to the time-dependent Schrödinger equation in the finite-dimensional form $\mathrm{i}\,\dot{U} = HU$ where H, the Hamiltonian, is a Hermitean matrix and U may be regarded as the unitary time-evolution operator. More conveniently, we may identify any column of U as a finite-dimensional wavefunction $|\psi\rangle$ and, as is well known, conservation of probability and unitarity of U follow from the Schrödinger equation. We discuss the application to quantum mechanics and the generalization to infinite dimensions elsewhere, by investigating the time-dependent Schrödinger equation on a quantum network with nonlinear network interactions leading to quantum synchronization.

In general, therefore, unitarity of all variables U_i follows from the requirement that the right-hand side of (2) be Hermitean, together with the initial conditions $U_i U_i^\dagger = I_n$, and so the system evolves with all trajectories restricted to the compact manifold of the unitary group. One can add further terms to the model such as self-interactions or network interactions, provided they are Hermitean, and the trajectories in all such cases are confined to the $U(n)$ manifold. A typical self-interaction is the linear term $\mathrm{i}\alpha(U_i - U_i^\dagger)$ which for the Abelian model reduces to $\alpha \sin\theta_i$ and may be added to the right-hand side of (1), where α is a coupling constant, as has been discussed for the Kuramoto model by Sakaguchi [16] (also with a forcing term) and others [14, 17]. Further network interactive terms could include $\mathrm{i}\sum_{j=1}^N a_{ij}(U_i^\dagger U_j - U_j^\dagger U_i)$ where the order of the noncommuting variables is reversed compared to (2), and other terms could include $\mathrm{i}\sum_{j=1}^N a_{ij}[(U_i U_j^\dagger)^m - (U_j U_i^\dagger)^m]$ for any positive integer m, or a sum of such terms over m, which would lead to generalizations of the models discussed in [7, see section V.A]. A consideration, however, for all such interactions is whether or not phase synchronization occurs. Numerical investigations (as in section 5) indicate that trajectories in such models are generally spatially synchronized (as discussed also in section 7.1) but because there is relative motion within synchronized clusters, phase locking does not necessarily occur. We discuss this specifically for the S^2 model in section 5, but for the models given by (2) we show in

section 3 that there do exist limit cycles and that phase locking can therefore occur. This is verified numerically for $n = 2$ in section 6.

Equations (2) are covariant under the simultaneous global transformations

$$U_i \to SU_iT, \qquad H_i \to SH_iS^\dagger, \tag{4}$$

where S, T are unitary time-independent matrices, independent of i. This constitutes a chiral (left–right) $SU(n) \times SU(n)$ covariance together with a $U(1)$ covariance, i.e. for any solutions U_i the variables SU_iT are also solutions provided that the matrices H_i transform as in (4). Accordingly, we refer to (2) as an $SU(n) \times SU(n)$ model.

The model (2) is a set of equations relating elements of the Lie algebra $\mathfrak{u}_n$ of $U(n)$ and extends to subgroups of $U(n)$. If the matrices H_i are elements of a subalgebra of $\mathfrak{u}_n$, and if each U_i is initially an element of the corresponding subgroup of $U(n)$, then the system evolves on the manifold of that subgroup. For example, if the $n \times n$ matrices $J_i = -\mathrm{i}H_i$ are all real and antisymmetric, and are therefore elements of the Lie algebra $\mathfrak{so}_n$, and if the initial matrices $U_i(0)$ are elements O_i of the rotation group $SO(n)$, then the variables $O_i(t)$ are restricted to the group manifold of $SO(n)$ for all subsequent times. We can state the equations for this model in the form

$$\dot{O}_iO_i^t = J_i - \frac{\kappa}{2N}\sum_{j=1}^{N} a_{ij}\,(O_iO_j^t - O_jO_i^t) \qquad (i = 1, \ldots, N), \tag{5}$$

where J_i is a given set of real, antisymmetric $n \times n$ matrices, the variables O_i are $n \times n$ real matrices and O^t denotes the transpose of O. Since all terms on the right-hand side of (5) are antisymmetric it follows as before that $O_iO_i^t$ is a constant of the motion at each node and so, by initially choosing $O_iO_i^t$ to be the identity matrix I_n, the variables O_i evolve as elements of $SO(n)$. For the Abelian case $n = 2$ with $J_i = -\nu_i\,\imath_2$ and $O_i = \mathrm{e}^{-\imath_2\theta_i}$, where

$$\imath_2 = \begin{pmatrix} 0 & -1 \\ 1 & 0 \end{pmatrix}, \qquad O_i = \begin{pmatrix} \cos\theta_i & \sin\theta_i \\ -\sin\theta_i & \cos\theta_i \end{pmatrix}, \tag{6}$$

we regain the Kuramoto equations (1). Equations (5) are covariant under $SO(n) \times SO(n)$ global transformations defined by

$$O_i \to SO_iT, \qquad J_i \to SJ_iS^t$$

where $S, T \in SO(n)$. We briefly discuss the $SO(3) \times SO(3)$ model in section 6. There also exist non-Abelian Kuramoto models for the symplectic groups, with defining equations similar to (5), and hence for all classical compact Lie groups. By choosing an indefinite metric one may extend these models to the noncompact case, for which trajectories are unbounded, however, we do not discuss synchronization or other properties of these particular models here. These models differ from those proposed in [18].

If the Hermitean matrices H_i mutually commute for all i they generate a $\mathfrak{u}_1 \oplus \cdots \mathfrak{u}_1$ subalgebra of $\mathfrak{u}_n$, and we may simultaneously diagonalize all H_i using the transformation (4) with a suitable unitary matrix S. If the initial matrices $U_i(0)$ are also chosen to be diagonal and are therefore elements of $U(1) \times \cdots U(1)$ then, by parametrizing each U_i as a diagonal unitary matrix, equations (2) decouple into n Abelian Kuramoto systems with a common coupling constant and synchronization occurs in the usual way. Trajectories are confined to the manifold $S^1 \times \cdots S^1$, with properties of the synchronized trajectories determined by the $\mathfrak{u}_1 \oplus \cdots \mathfrak{u}_1$ subalgebra of $\mathfrak{u}_n$.

The question arises therefore in general as to the possible trajectories of the system if the matrices H_i belong to a subalgebra $\mathfrak{a}$ of $\mathfrak{u}_n$, but for which the initial matrices $U_i(0)$ are general unitary matrices with elements chosen at random, not necessarily elements of the

subgroup corresponding to $\mathfrak{a}$. Numerical investigations described in later sections indicate that in this case synchronized trajectories have properties, such as common frequencies, that are independent of the initial conditions and are determined by the specific algebra $\mathfrak{a}$, i.e. synchronized trajectories are confined to the group manifold corresponding to $\mathfrak{a}$ for any initial conditions. For the $SU(2) \times SU(2)$ model investigated in section 6 we find numerically for the general synchronized solution, with sufficiently large κ and all-to-all coupling, that trajectories are bunched together on the group manifold of $SU(2)$, namely S^3, with each trajectory following a unit circle on S^3 but with such circles slightly tilted with respect to each other. For the Abelian case with commuting H_i, however, these synchronized unit circles are coplanar, and so all trajectories are confined to a common unit circle as for the Abelian Kuramoto model; the orientation of this common circle depends, however, on the initial conditions. We find a similar property for the S^2 model discussed in section 5, where trajectories for the particular Abelian case resemble those of the Abelian Kuramoto model, in that all synchronized particles are approximately aligned on S^2 in a linear formation resembling S^1 trajectories.

Synchronization may be measured as for the Abelian Kuramoto model by means of an order matrix R defined by

$$R\,V = \frac{1}{N}\sum_{j=1}^{N} U_j, \tag{7}$$

where we have expressed the sum as a left polar decomposition, where R is a positive semidefinite Hermitean matrix and V is unitary. The eigenvalues of R, which lie between zero and unity, may be regarded as order parameters with values close to unity signifying synchronization for corresponding modes of oscillation. Under the global transformation (4) we have $R \to SRS^\dagger$ and so R can be diagonalized by a suitable choice of S.

For the case of all-to-all coupling we can write the defining equations (2) in terms of the order matrix and each U_i may be regarded, as in the Abelian case, as coupling to a mean field quantity RV. We investigate this more fully in section 7 where we express the order parameter in terms of the centre-of-mass coordinate $\boldsymbol{x}_{\text{CM}}$, defined as the average location of all particles $\boldsymbol{x}_i$, to which each particle couples.

3. Non-Abelian limit cycles

The Abelian Kuramoto equations (1) are solved by the limit cycle $\theta_i(t) = \theta_i^0 + \lambda t$ where the synchronized frequency λ is the mean of the frequencies ν_i, and where the constants θ_i^0 satisfy corresponding nonlinear algebraic equations. Hence, this phase-locked solution oscillates at each node like a free system but with the natural frequency replaced by the common synchronized frequency λ. This limit cycle generalizes for the non-Abelian case to

$$U_i(t) = u_i\, \mathrm{e}^{-\mathrm{i}\Lambda t}, \tag{8}$$

where u_i is a constant $n \times n$ unitary matrix, and Λ is a constant $n \times n$ Hermitean matrix, and is therefore an element of $\mathfrak{u}_n$. We refer to (8) as a 'limit cycle' because numerical investigations indicate that synchronized trajectories are numerically indistinguishable from these solutions, following an initial transient. Equations (2) are satisfied provided

$$\Lambda - \widetilde{H}_i = -\frac{\mathrm{i}\kappa}{2N}\sum_{j=1}^{N} a_{ij}\left(u_j^\dagger u_i - u_i^\dagger u_j\right), \tag{9}$$

where the Hermitean matrix $\widetilde{H}_i = u_i^\dagger H_i u_i$ has the same eigenvalues (natural frequencies) as H_i. The solution (8) compares with the free solution (for $\kappa = 0$) at each node,

$U_i(t) = \mathrm{e}^{-\mathrm{i}H_i t}u_i = u_i\,\mathrm{e}^{-\mathrm{i}\widetilde{H}_i t}$, where u_i is a constant unitary matrix. In the free case each node oscillates as a linear superposition of the natural modes of oscillation, as determined by the eigenvalues of H_i or $\widetilde{H}_i$, whereas when synchronized each node oscillates as a linear superposition of the synchronized modes of oscillation determined by Λ, independent of i.

It follows from (9), by taking the matrix 2-norm $\|.\|$ of both sides, that

$$\|\Lambda - \widetilde{H}_i\| \leqslant \frac{\kappa}{N}\sum_{j=1}^{N}|a_{ij}|, \tag{10}$$

where we have used the triangle inequality and the fact that $\|u\| = 1$ for any unitary matrix u. For properties of the matrix 2-norm see [19] (chapter 1), in particular we have $\|Z\| = \sqrt{\rho(Z^\dagger Z)}$ for any square matrix Z, where the spectral radius ρ is defined by $\rho(Z) = \max_s |\lambda_s(Z)|$, where $\lambda_s(Z)$ denotes the sth eigenvalue of Z. It follows that $\|uZv\| = \|Z\|$ for any unitary matrices u, v. For example, we have from (7), by means of the triangle inequality, that $\|R\| \leqslant 1$ and hence that the maximum eigenvalue of R is less than unity.

The inequality (10) is a necessary condition for the limit cycle (8) to satisfy (2) and states that the natural frequencies at each node must be near the synchronized frequencies for synchronization to occur, and that therefore κ or the ratio $\sum_{j=1}^{N} a_{ij}/N$, which is the average number of connections to the node i, must be sufficiently large. If the inequality (10) is violated at some nodes then partial synchronization occurs, similar to that for the Abelian model, as is demonstrated by numerical calculations.

How is the synchronization matrix Λ determined? Since the inequalities (10) must be satisfied for all i one might expect Λ to minimize $\sum_i \|\Lambda - \widetilde{H}_i\|^2$ which, as discussed in section 7.2, agrees with numerical evaluations of Λ. Given any synchronized solution $U_i(t)$ we therefore determine Λ by minimizing the function F defined by

$$F(\Lambda) = \frac{1}{N}\sum_{i=1}^{N}\|U_i(t)\Lambda - H_i U_i(t)\|^2 \tag{11}$$

with respect to Λ, at any fixed time t following synchronization, however a proof that Λ is determined in this way requires a stability analysis of the fixed point solutions. For the Abelian Kuramoto model, for which $H_i = \nu_i$ and $\Lambda = \lambda$, we have $F(\lambda) = \sum_i(\nu_i - \lambda)^2/N$ at any time, and the minimum of F occurs at $\lambda = \sum_i \nu_i/N$. In general, Λ depends on κ, on the natural frequencies of H_i, and also on the initial values $U_i(0)$ but for the cases explicitly investigated, the synchronized frequency of the trajectories is independent of $U_i(0)$. There appears to be no simple formula which in general relates the synchronized frequencies to H_i and κ.

In discussing a range of models in the following we find it necessary to distinguish between spatial and phase synchronization. The order parameter R defined in (7) measures the spatial synchronization of the system, but not whether trajectories are phase-locked, i.e. whether (8) is a limit cycle. As discussed in sections 5.1, 6.1 and also in [14], phase-locked solutions can exist independent of spatial synchronization. If the solution $U_i(t)$ is phase-locked, Λ may be determined by minimizing F defined by (11), and then one may verify numerically that (8) is a limit cycle by evaluating, after synchronization has occurred, the time-dependent parameter

$$\frac{1}{N}\sum_{i=1}^{N}\|\mathrm{i}\dot{U}_i(t) - U_i(t)\Lambda\|$$

which is zero for solutions (8). Alternatively, in order to avoid the numerical computation of time derivatives, one can evaluate

$$\frac{1}{N}\sum_{i=1}^{N}\|\mathrm{i}\,U_i(t+1) - U_i(t)\,\mathrm{e}^{-\mathrm{i}\Lambda}\|, \tag{12}$$

which is also zero for the limit cycle (8).

If the solution $U_i(t)$ is not phase-locked then the degree of phase synchronization can be measured by disorder parameters defined independently of Λ. One measure follows from the observation that $U_i U_j^\dagger$ is constant for any pair i, j for (8) and hence the following sum, averaged over all pairs i, j,

$$D^{(1)}(t) = \frac{2}{N(N-1)} \sum_{i<j} \left\| \frac{\mathrm{d}}{\mathrm{d}t} \left(U_i(t) U_j^\dagger(t) \right) \right\|, \tag{13}$$

is a measure of phase disorder, and is zero within numerical error for a phase-locked system. The time derivative in this expression may be evaluated numerically by a finite difference over a small interval. For the Abelian case, in which $U_i = \mathrm{e}^{-\mathrm{i}\theta_i}$, $D^{(1)}(t)$ measures the average frequency separation between all pairs of nodes.

A zero value for $D^{(1)}$, however, establishes only that $U_i U_j^\dagger$ is constant for any pair i, j, and hence that $U_i(t) = u_i\, \mathrm{e}^{-\mathrm{i}A(t)}$ for a constant unitary matrix u_i and for some time-dependent Hermitean matrix $A(t)$ independent of i. A second method of measuring phase locking follows from the observation that for (8) we have $\|\dot{U}_i(t)\| = \|\Lambda\|$, that is, for a phase-locked solution $\|\dot{U}_i(t)\|$ is independent of both i and t, with a value equal to the largest synchronized frequency. We therefore define a second disorder measure

$$D^{(2)}(t) = \frac{2}{N(N-1)} \sum_{i<j} |(\|\dot{U}_i(t)\| - \|\dot{U}_j(t)\|)|, \tag{14}$$

then a zero value for $D^{(2)}$ implies that $\|\dot{U}_i(t)\|$ is independent of i and t and hence, assuming $U_i(t) = u_i\, \mathrm{e}^{-\mathrm{i}A(t)}$, that $\|\dot{U}_i(t)\| = \|\dot{A}\|$ is time independent which in turn implies that $\dot{A}$ is constant in time. Therefore we establish the existence of phase-locked synchronization, without explicit knowledge of Λ, by verifying numerically that both disorder measures $D^{(1)}(t)$ and $D^{(2)}(t)$ are zero for all times beyond the initial transient time; if the solution $U_i(t)$ is not phase-locked then $D^{(1)}$, $D^{(2)}$ provide measures of the phase disorder.

4. The $U(2) \times U(2)$ model and the $(m-1)$-sphere models

Consider now equations (2) for $n = 2$, and parametrize the unitary matrix U_i in the usual way in terms of a real 4-vector $\boldsymbol{x}_i = (x_i^1, x_i^2, x_i^3, x_i^4)$ according to

$$U_i = \mathrm{e}^{-\mathrm{i}\theta_i} \left(\mathrm{i} \sum_{k=1}^{3} x_i^k \sigma_k + x_i^4\, I_2 \right) = \mathrm{e}^{-\mathrm{i}\theta_i} \begin{pmatrix} x_i^4 + \mathrm{i}x_i^3 & x_i^2 + \mathrm{i}x_i^1 \\ -x_i^2 + \mathrm{i}x_i^1 & x_i^4 - \mathrm{i}x_i^3 \end{pmatrix}, \tag{15}$$

where $\{\sigma_k\}$ denotes the Pauli σ-matrices. This parametrization expresses U_i as a product of a phase $\mathrm{e}^{-\mathrm{i}\theta_i}$ and an $SU(2)$ matrix provided $\|\boldsymbol{x}_i\| = 1$, however, we allow $\boldsymbol{x}_i$ to be unconstrained and then the equations of motion enforce $\|\boldsymbol{x}_i\| = 1$ as a constant of the motion for each i. We expand H_i in terms of a basis of $\mathfrak{u}_2$ according to

$$H_i = \sum_{k=1}^{3} \omega_i^k \sigma_k + \nu_i\, I_2, \tag{16}$$

where $\boldsymbol{\omega}_i = (\omega_i^1, \omega_i^2, \omega_i^3)$ is a real 3-vector and the frequency ν_i is associated with the $U(1)$ component of U_i. After substitution into (2) and following algebraic manipulations we obtain $5N$ equations for the angles θ_i and the 4-vectors $\boldsymbol{x}_i$:

$$\|\boldsymbol{x}_i\|^2\, \dot{\theta}_i = \nu_i + \frac{\kappa}{N} \sum_{j=1}^{N} a_{ij}\, \sin(\theta_j - \theta_i)\, \boldsymbol{x}_i \cdot \boldsymbol{x}_j\,, \tag{17}$$

$$\|\boldsymbol{x}_i\|^2\,\dot{\boldsymbol{x}}_i = \Omega_i\,\boldsymbol{x}_i + \frac{\kappa}{N}\sum_{j=1}^{N} a_{ij}\cos(\theta_j-\theta_i)\left(\|\boldsymbol{x}_i\|^2\,\boldsymbol{x}_j - \boldsymbol{x}_i\cdot\boldsymbol{x}_j\,\boldsymbol{x}_i\right), \tag{18}$$

where Ω_i is the real 4×4 antisymmetric matrix

$$\Omega_i = \begin{pmatrix} 0 & -\omega_i^3 & \omega_i^2 & -\omega_i^1 \\ \omega_i^3 & 0 & -\omega_i^1 & -\omega_i^2 \\ -\omega_i^2 & \omega_i^1 & 0 & -\omega_i^3 \\ \omega_i^1 & \omega_i^2 & \omega_i^3 & 0 \end{pmatrix}. \tag{19}$$

It follows from (18) by using the antisymmetry of Ω_i that $\boldsymbol{x}_i\cdot\dot{\boldsymbol{x}}_i = 0$ and hence that $\|\boldsymbol{x}_i\|$ is a constant of the motion for each i. As previously discussed, we choose initial conditions such that $U_i(0)$ is unitary and hence $\|\boldsymbol{x}_i(0)\| = 1$ for each i, which implies $\|\boldsymbol{x}_i\| = 1$ for all subsequent times. Henceforth we set the factors $\|\boldsymbol{x}_i\|^2$ equal to unity on the left-hand sides of equations (17), (18), although it is useful to explicitly retain the factor $\|\boldsymbol{x}_i\|^2$ on the right-hand side of (18), since then $\boldsymbol{x}_i\cdot\dot{\boldsymbol{x}}_i = 0$ follows immediately. The value $\|\boldsymbol{x}_i\| = 1$ is nevertheless maintained as a constant of the motion by setting $\|\boldsymbol{x}_i\| = 1$ on the right-hand side of (18), since then

$$\boldsymbol{x}_i\cdot\dot{\boldsymbol{x}}_i = \frac{\kappa}{N}\left(1-\|\boldsymbol{x}_i\|^2\right)\sum_{j=1}^{N} a_{ij}\cos(\theta_j-\theta_i)\boldsymbol{x}_i\cdot\boldsymbol{x}_j,$$

which implies that if $\|\boldsymbol{x}_i\|^2 = 1$ initially then $\|\boldsymbol{x}_i\|^2 = 1$ also for all subsequent times. This also appears to have numerical advantages in terms of accuracy. Equations (17) and (18) may be integrated numerically without difficulty by standard routines, with the accuracy of integration evaluated by calculating the total error $\sum_i |(\|\boldsymbol{x}_i\| - 1)|$ at the final time.

In summary, the equations of motion (17),(18) for the unconstrained variables $\theta_i, \boldsymbol{x}_i$ restrict all trajectories to lie on the $U(2)$ group manifold $S^1\times S^3$. Consider now specifically the $SU(2)$ case by choosing $\nu_i = 0$ for all i in which case H_i is an element of the Lie algebra $\mathfrak{su}_2$. We may then satisfy (17) by setting $\theta_i = 0$ and write the remaining $4N$ equations of motion in the form

$$\dot{\boldsymbol{x}}_i = \Omega_i\,\boldsymbol{x}_i + \frac{\kappa}{N}\sum_{j=1}^{N} a_{ij}\left(\|\boldsymbol{x}_i\|^2\,\boldsymbol{x}_j - \boldsymbol{x}_i\cdot\boldsymbol{x}_j\,\boldsymbol{x}_i\right), \qquad (i=1,\ldots,N). \tag{20}$$

As derived, $\boldsymbol{x}_i$ is a 4-vector but we now generalize these equations by allowing $\boldsymbol{x}_i$ to be an m-vector in $\mathbb{R}^m$, and Ω_i to be a set of real, antisymmetric $m\times m$ matrices. Equations (20) therefore consist of mN equations for the mN variables $\boldsymbol{x}_i$. As before, we deduce that $\boldsymbol{x}_i\cdot\dot{\boldsymbol{x}}_i = 0$ and hence that $\|\boldsymbol{x}_i\|$ is constant for each i, and so by initially choosing $\|\boldsymbol{x}_i\| = 1$ we find that all trajectories lie on S^{m-1}. This property is maintained if we allow self-interactions at each node by allowing Ω_i to depend on $\boldsymbol{x}_i$, possibly also with a given time dependence, provided only that Ω_i be antisymmetric. By including the $U(1)$ component as in (17) all trajectories lie on $S^1\times S^{m-1}$.

Equations (20) for general m provide another generalization of the Abelian Kuramoto model since for $m = 2$ we regain equations (1), as is evident upon choosing $\Omega_i = \nu_i\,\iota_2$ where ι_2 is defined in (6), and parametrizing the unit 2-vectors according to $\boldsymbol{x}_i = (\cos\theta_i\,,\sin\theta_i)$. For general $m\neq 2, 4$ these models differ, however, from the $SU(n)\times SU(n)$ models (2) although they may be related by the addition of symmetry-breaking terms in the defining equations, as we discuss for $m = 3$ in the following section.

Whereas equations (2) are covariant with respect to $SU(n)\times SU(n)$, equations (20) are covariant with respect to $SO(m)$, since for any $O\in SO(m)$ and any solution $\boldsymbol{x}_i$ the vector

$O\boldsymbol{x}_i$ is also a solution, provided Ω_i is replaced by $O\Omega_i O^t$ (hence Ω_i transforms as a rank-2 tensor under rotations). For $m = 4$ this global covariance corresponds to the covariance (4), as follows from the local isomorphism $SO(4) \cong SU(2) \times SU(2)$. Accordingly, we refer to (20) as the $SO(m)$, or $(m-1)$-sphere model. One can generalize this model to $U(m)$ where the covariance group is $U(m)$ and the variables are complex m-vectors $\boldsymbol{z}_i$, however since this model is relevant to quantum-mechanical applications we discuss it elsewhere.

For zero coupling $\kappa = 0$ in (20) each node oscillates at its natural frequency as determined by $\dot{\boldsymbol{x}}_i = \Omega_i \boldsymbol{x}_i$, which implies $\ddot{\boldsymbol{x}}_i = (\Omega_i)^2 \boldsymbol{x}_i$. Since Ω_i is antisymmetric all eigenvalues of $-(\Omega_i)^2$ are nonnegative, but for odd m there exists at least one zero eigenvalue and a corresponding zero frequency mode of oscillation. The oscillating solutions are given by $\boldsymbol{x}_i(t) = \mathrm{e}^{t\,\Omega_i}\boldsymbol{n}_i$ where $\boldsymbol{n}_i = \boldsymbol{x}_i(0)$ is a constant unit vector.

We discuss the case $m = 3$ in the following section, for which trajectories lie on S^2 and is of particular interest, however, generally we find that trajectories in these models synchronize spatially but are not necessarily phase-locked. We define the order parameter $r(t)$, following Kuramoto [13] and consistent with the definition (7), by first defining the centre-of-mass vector $\boldsymbol{x}_{\mathrm{CM}}$, geometrically the centroid,

$$\boldsymbol{x}_{\mathrm{CM}} = \frac{1}{N}\sum_{j=1}^{N} \boldsymbol{x}_j, \tag{21}$$

where we regard $\boldsymbol{x}_i$ as the location of a particle of unit mass. Then the parameter $r(t) = \|\boldsymbol{x}_{\mathrm{CM}}(t)\|$, which lies between zero and unity, measures the spatial coherence of the trajectories. Whether phase locking occurs, however, depends on the choice of $\Omega_i \in \mathfrak{so}_m$. A limit cycle solution takes the form

$$\boldsymbol{x}_i(t) = \mathrm{e}^{t\,\Lambda}\boldsymbol{n}_i, \tag{22}$$

where Λ is a constant real $m \times m$ antisymmetric matrix, i.e. an element of $\mathfrak{so}_m$, and $\boldsymbol{n}_i$ is a constant unit m-vector at the node i. Equations (20) are satisfied provided $[\Omega_i, \Lambda] = 0$ for all i and

$$(\Lambda - \Omega_i)\boldsymbol{n}_i = \frac{\kappa}{N}\sum_{j=1}^{N} a_{ij}(\boldsymbol{n}_j - \boldsymbol{n}_i \cdot \boldsymbol{n}_j \boldsymbol{n}_i),$$

which constitutes a set of nonlinear algebraic equations for $\boldsymbol{n}_i$. Corresponding to (10) we have

$$\|(\Lambda - \Omega_i)\boldsymbol{n}_i\| \leqslant \frac{2\kappa}{N}\sum_{j=1}^{N} |a_{ij}|,$$

which shows that phase locking occurs only under certain conditions such as sufficiently large values of κ.

For $m = 2$ we have $\Omega_i = \nu_i\, \iota_2$ and $\Lambda = \lambda\, \iota_2$ for the synchronized frequency $\lambda = \sum_i \nu_i/N$, where ι_2 is defined in (6), and so $[\Omega_i, \Lambda] = 0$ is satisfied for all i. In general, the Lie algebra spanned by the generators Ω_i must commute with the Lie algebra to which Λ belongs, for a limit cycle and hence phase locking to exist. For $m = 4$, in which case $SO(4) \cong SU(2) \times SU(2)$, Ω_i and Λ are elements of the respective commuting $\mathfrak{su}_2$ algebras, and so a limit cycle exists and phase locking can occur, as we discuss in section 6.

Whereas spatial synchronization is measured by the order parameter r, partial phase synchronization may be measured by one or more disorder parameters related to those defined in (13) and (14). Since $\boldsymbol{x}_i \cdot \boldsymbol{x}_j$ is constant for all pairs of nodes i, j, as follows from (22), or

equivalently the distance $\|\boldsymbol{x}_i - \boldsymbol{x}_j\|$ between any two nodes is constant, the averaged disorder measure

$$d^{(1)}(t) = \frac{2}{N(N-1)} \sum_{i<j} \left| \frac{\mathrm{d}}{\mathrm{d}t} \left(\boldsymbol{x}_i \cdot \boldsymbol{x}_j \right) \right| \tag{23}$$

is zero for phase-locked trajectories, i.e. for the limit cycle (22). A related measure, as discussed in section 3, follows by observing that for limit cycles (22) the quantity $\|\dot{\boldsymbol{x}}_i(t)\| = \|\Lambda\, \boldsymbol{n}_i\|$ is constant in time.

For phase-locked trajectories $\boldsymbol{x}_i(t)$ the matrix Λ can be determined, following the definition (11) and as discussed also in section 7.2, by minimizing

$$F(\Lambda) = \frac{1}{N} \sum_{i=1}^{N} \|(\Omega_i - \Lambda)\boldsymbol{x}_i\|^2 \tag{24}$$

with respect to Λ, at any time following synchronization. Then $\sum_i \|\dot{\boldsymbol{x}}_i(t) - \Lambda \boldsymbol{x}_i(t)\|$ should numerically be equal to zero for all times following synchronization, since synchronized trajectories satisfy $\dot{\boldsymbol{x}}_i = \Lambda \boldsymbol{x}_i$. Another test of phase locking is to evaluate the measure corresponding to (12),

$$d(t) = \frac{1}{N} \sum_{i=1}^{N} \|\boldsymbol{x}_i(t+1) - \mathrm{e}^{\Lambda} \boldsymbol{x}_i(t)\|, \tag{25}$$

which does not involve time derivatives, and is zero at all times following synchronization. We discuss the application of these measures to the $SU(2) \times SU(2)$ model in section 6.

5. The 2-sphere model

Consider now the S^2 model consisting of equations (20) for the 3-vectors $\boldsymbol{x}_i$, possibly with a $U(1)$ coupling as in (17). This model differs from the tops model considered in [20], also discussed in [7, section V.B], in that the restriction of trajectories to S^2 is not imposed by an external constraint but is a consequence of the equations of motion. This model may be formulated, analogous to equations (2), as the $n = 2$ case of $n \times n$ unitary matrices U_i at each node which satisfy

$$\mathrm{i}\, \dot{U}_i U_i^\dagger = \nu_i\, I_n + H_i - U_i H_i U_i^\dagger - \frac{\mathrm{i}\kappa}{2N} \sum_{j=1}^{N} a_{ij} \left(U_i U_j^\dagger - U_j U_i^\dagger \right), \tag{26}$$

where ν_i denotes the frequency corresponding to the Abelian component of U_i, and $\{H_i\}$ is a given set of $n \times n$ Hermitean matrices in $\mathfrak{su}_n$, with zero trace. Since the right-hand side of (26) is Hermitean, U_i is unitary for each i provided that each U_i is initially chosen to be unitary. The global covariance (4) is valid only for $S = T$, and so (26) is covariant under unitary global transformations. These equations constitute another non-Abelian generalization of the Kuramoto equations (1), to which they reduce for $n = 1$. Generally, however, phase-locked synchronization occurs only under restricted conditions, in particular for the limit cycle (8) to satisfy (26) it is necessary that $[H_i, \Lambda] = 0$ for all i, a condition consistent with that found for the limit cycle (22) for the S^{m-1} model.

Consider now $n = 2$ and set H_i to be the $\mathfrak{su}_2$ element $H_i = \boldsymbol{\omega}_i \cdot \boldsymbol{\sigma}/2$, where $\boldsymbol{\omega}_i = (\omega_i^1, \omega_i^2, \omega_i^3)$ and $\boldsymbol{\sigma} = (\sigma_1, \sigma_2, \sigma_3)$. We parametrize U_i according to

$$U_i = \mathrm{e}^{-\mathrm{i}\theta_i} \begin{pmatrix} \mathrm{i}\, x_i^3 & x_i^2 + \mathrm{i}\, x_i^1 \\ -x_i^2 + \mathrm{i}\, x_i^1 & -\mathrm{i}\, x_i^3 \end{pmatrix}, \tag{27}$$

which is obtained by setting $x_i^4 = 0$ in (15), then we find equations (26) are satisfied provided (17,18) hold, where $\boldsymbol{x}_i = (x_i^1, x_i^2, x_i^3)$ is now a unit 3-vector and the real antisymmetric matrix Ω_i is given by

$$\Omega_i = \begin{pmatrix} 0 & -\omega_i^3 & \omega_i^2 \\ \omega_i^3 & 0 & -\omega_i^1 \\ -\omega_i^2 & \omega_i^1 & 0 \end{pmatrix}. \tag{28}$$

Evidently equations (26) preserve the zero trace property of U_i as parametrized in (27). We also set $\nu_i = 0$ for all i together with $\theta_i = 0$, in which case we regain (20) for $m = 3$. It is convenient to write these equations in the 3-vector form

$$\dot{\boldsymbol{x}}_i = \boldsymbol{\omega}_i \times \boldsymbol{x}_i + \frac{\kappa}{N} \sum_{j=1}^{N} a_{ij} (\|\boldsymbol{x}_i\|^2 \boldsymbol{x}_j - \boldsymbol{x}_i \cdot \boldsymbol{x}_j \, \boldsymbol{x}_i), \tag{29}$$

which imply $\dot{\boldsymbol{x}}_i \cdot \boldsymbol{x}_i = 0$.

Natural oscillations at each node are determined by the eigenvalues of $-(\Omega_i)^2$, namely $\{0, \|\boldsymbol{\omega}_i\|^2, \|\boldsymbol{\omega}_i\|^2\}$. The generic equations $\dot{\boldsymbol{x}} = \boldsymbol{\omega} \times \boldsymbol{x}$ for the free case have the solution

$$\boldsymbol{x}(t) = \boldsymbol{m} \, \sin\phi \, \cos\omega t + \boldsymbol{n} \, \sin\phi \, \sin\omega t + \widehat{\boldsymbol{\omega}} \, \cos\phi, \tag{30}$$

where ϕ is a constant angle, $\omega = \|\boldsymbol{\omega}\|$, and $\widehat{\boldsymbol{\omega}}$ is the unit vector defined by $\widehat{\boldsymbol{\omega}} = \boldsymbol{\omega}/\|\boldsymbol{\omega}\|$, and where $\{\widehat{\boldsymbol{\omega}}, \boldsymbol{n}, \boldsymbol{m}\}$ is a set of mutually orthogonal unit vectors satisfying

$$\boldsymbol{n} = \widehat{\boldsymbol{\omega}} \times \boldsymbol{m}, \quad \boldsymbol{m} = \boldsymbol{n} \times \widehat{\boldsymbol{\omega}}, \quad \widehat{\boldsymbol{\omega}} = \boldsymbol{m} \times \boldsymbol{n}.$$

If the initial conditions are such that $\phi = 0$ or $\phi = \pi$ then $\boldsymbol{x}$ remains stationary at the fixed point solution $\pm\widehat{\boldsymbol{\omega}}$, whereas if $\phi = \pi/2$ the trajectory lies on the equator with respect to the poles $\pm\widehat{\boldsymbol{\omega}}$, with a frequency ω of oscillation. For general initial conditions the free motion at each node is therefore a linear superposition of these two modes, and so trajectories lie on a circle of fixed latitude with respect to the poles $\pm\widehat{\boldsymbol{\omega}}$, with a frequency $\omega = \|\boldsymbol{\omega}\|$.

One expects spatially synchronized solutions of the coupled equations (29) to display similar behaviour, in which the cluster of particles is confined to a fixed latitude with a synchronized frequency λ. Hence the unit centre-of-mass vector $\widehat{\boldsymbol{x}}_{\rm CM} = \boldsymbol{x}_{\rm CM}/\|\boldsymbol{x}_{\rm CM}\|$, where $\boldsymbol{x}_{\rm CM}$ is defined in (21), should satisfy (30) with ω replaced by λ. Numerically we find, however, that $\widehat{\boldsymbol{x}}_{\rm CM}$ is generally not restricted to a fixed latitude but drifts to one of the poles $\pm\widehat{\boldsymbol{\omega}}$ in circles of decreasing radius. However, let us consider first the possible limit cycles.

As discussed in the previous section, the limit cycle (22) requires the existence of an antisymmetric matrix Λ such that $[\Omega_i, \Lambda] = 0$ for all i. For general Ω_i such a matrix does not exist, however if Ω_i belongs to an $\mathfrak{so}_2$ subalgebra of $\mathfrak{so}_3$, which occurs for example if two of the three frequencies $(\omega_i^1, \omega_i^2, \omega_i^3)$ are zero for all i, then Ω_i and Λ are proportional to an $\mathfrak{so}_2$ generator, and therefore commute for all i. To be specific, choose $\omega_i^1 = 0 = \omega_i^2$ for all i, then $\Omega_i = \omega_i^3 \, \iota_3$ and $\Lambda = \lambda \, \iota_3$ where

$$\iota_3 = \begin{pmatrix} 0 & -1 & 0 \\ 1 & 0 & 0 \\ 0 & 0 & 0 \end{pmatrix}.$$

The limit cycle (22), consistent with the natural oscillations (30), is given explicitly by

$$\boldsymbol{x}_i(t) = \mathrm{e}^{t\,\Lambda} \boldsymbol{n}_i = \big(n_i^1, n_i^2, 0\big) \cos\lambda t + \big(-n_i^2, n_i^1, 0\big) \sin\lambda t + (0, 0, n_i^3), \tag{31}$$

where $\boldsymbol{n}_i$ is a unit 3-vector.

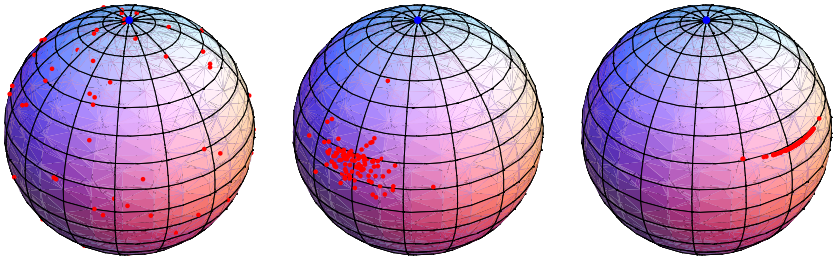

Figure 1. The locations on the unit sphere of the $N = 100$ particles for $\kappa = 2$ showing random positions at the initial time $t = 0$, partial synchronization at $t = 3$ and full synchronization at $t = 6.7$.

For the frequencies $\omega_i^1 = 0 = \omega_i^2$ the full equations (29) have the fixed point solution $\boldsymbol{x}_i = \pm(0, 0, 1)$ for any κ, corresponding to $\phi = 0$ or $\phi = \pi$ in the solution (30) of the free equations, i.e. $n_i^1 = 0 = n_i^2$ in the limit cycle (31). We may also satisfy (29) by setting $x_i^3 = 0$ for all i, in which case the equations reduce to those of the Abelian Kuramoto model. Hence, if the initial conditions are such that $\boldsymbol{x}_i(0)$ lies on the equator for all i, then all trajectories remain on the equator and synchronization occurs as for the Abelian Kuramoto model, in particular phase locking occurs, corresponding to $n_i^3 = 0$ in (31). For random initial conditions the trajectories not only spatially synchronize, as measured by the order parameter $r = \|\boldsymbol{x}_{\rm CM}\|$, but for sufficiently large κ all particles are spatially ordered in an almost linear array as for the Abelian Kuramoto model and are almost phase-locked.

We have solved (29) numerically for $\kappa = 2$ and $N = 100$ particles with a Gaussian distribution for the frequencies ω_i^3 about a mean $\omega = 2$, with a standard deviation 0.3, and an initial uniform random distribution of particles on S^2. Figure1 shows the N particles initially distributed randomly on S^2, followed by partial synchronization at $t = 3$ and full synchronization at $t = 6.7$ (corresponding to a constant value of r near unity). Evidently the particles when synchronized are aligned in an almost linear formation approximately along a fixed latitude. Figure 2 shows the trajectory of the unit centre of mass $\widehat{\boldsymbol{x}}_{\rm CM}$ for $0 \leqslant t \leqslant 60$. The cluster of particles spirals towards the fixed point $(0, 0, 1)$ as t increases, as indicated by the trajectory of $\widehat{\boldsymbol{x}}_{\rm CM}$ and the particle locations, shown at times $t = 22$ and $t = 60$, maintain the linear alignment even though the average particle separation decreases.

In figure 3, we plot the order parameter $r(t)$, showing that synchronization occurs at about $t = 4$ units when r takes a value close to unity which is almost constant. The disorder measure $d^{(1)}(t)$ of phase locking, defined in (23), is close to zero after $t = 4$ units, which demonstrates that trajectories are almost phase-locked following spatial synchronization at $t = 4$. A slight increase in $r(t)$ with t is visible in figure 3, specifically there is an increase of about 0.8% from $r \approx 0.9913$ at $t = 10$ to $r \approx 0.9992$ at $t = 60$, which is due to tighter bunching of particles as the cluster nears the pole $(0, 0, 1)$, as is evident also in figure 2. This demonstrates that phase locking is not 'exact', i.e. that the pairs $\boldsymbol{x}_i \cdot \boldsymbol{x}_j$ for all i, j are in fact slowly varying as the system evolves. Since $\|\boldsymbol{x}_i - \boldsymbol{x}_j\|^2 = 2 - 2\boldsymbol{x}_i \cdot \boldsymbol{x}_j$, a decreasing spatial separation $\|\boldsymbol{x}_i - \boldsymbol{x}_j\|$ for each pair i, j, and hence increasing $r(t)$, is associated with increasing values $\boldsymbol{x}_i \cdot \boldsymbol{x}_j$. The failure of exact phase locking, despite the existence of a 'limit cycle' (31), can be attributed therefore to the tendency of the particle cluster to drift towards a pole as time increases. This is confirmed by numerical calculation of other disorder parameters, such as that defined in (14) which is also small but nonzero following spatial synchronization. As further confirmation of this effect, one may calculate the frequency λ for the function (31) at any fixed time t by minimizing $\sum_i \|\dot{\boldsymbol{x}}_i(t) - \lambda t_3 \boldsymbol{x}_i(t)\|^2$ with respect to λ; we find that the

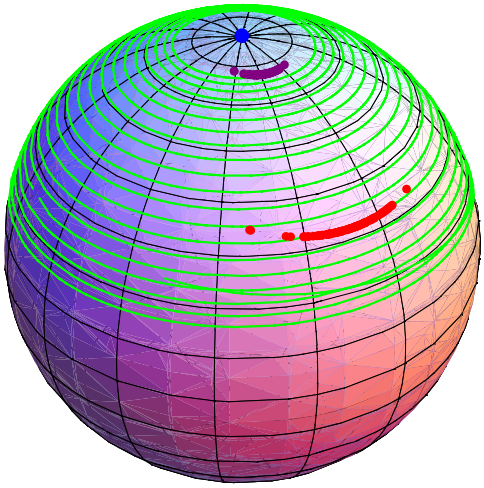

Figure 2. The trajectory of the unit centre-of-mass vector $\widehat{x}_{\rm CM}(t)$ for $0 \leqslant t \leqslant 60$ (green) traces out a spiral curve which is attracted to the pole (blue). The $N = 100$ particles are shown at time $t = 22$ (red) and $t = 60$ (purple), and maintain an alignment approximately along a fixed latitude.

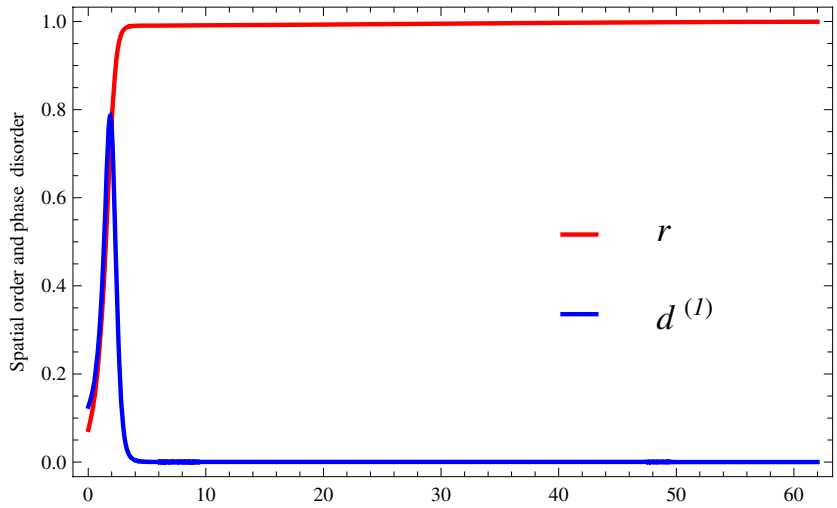

Figure 3. The order parameter r shows that spatial coherence for the system shown in figures 1 and 2 is achieved at about $t = 4$ units and phase locking, attained when the disorder parameter $d^{(1)}(t)$ is zero, occurs for $t > 4$.

minimum is small ($\approx$0.02), but not zero, and that λ is close but not equal to $\sum_i \omega_i^3/N$ with a more significant difference as the trajectories approach the pole.

Next we consider the general case in which the frequencies $\boldsymbol{\omega}_i = (\omega_i^1, \omega_i^2, \omega_i^3)$ are all nonzero and are distributed about mean values, choosing in our numerical examples Gaussian distributions of standard deviation 0.3 about $\boldsymbol{\omega} = (-2, 1, 2)$, again for $N = 100$ and $\kappa = 2$. The matrices Ω_i, which span the Lie algebra $\mathfrak{so}_3$, no longer commute for different i. We find numerically that after an initial transient time spatial synchronization occurs as before, as indicated by a value of $r(t)$ which is constant and close to unity. The N particles bunch

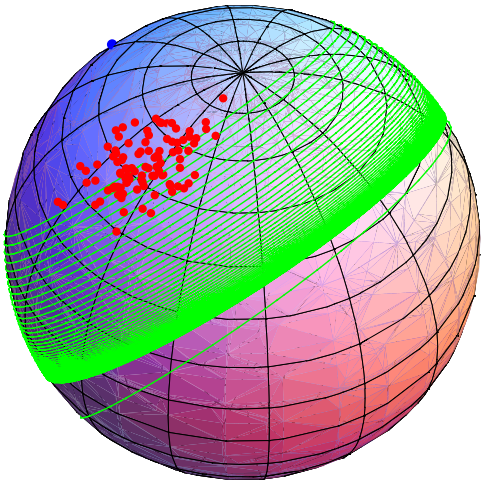

Figure 4. The trajectory of the unit centre-of-mass vector $\widehat{x}_{\rm CM}(t)$ for $0 \leqslant t \leqslant 120$ (green) drifts towards the pole (blue) located at $\widehat{\omega}$. The particle cluster (red) is shown at $t = 120$.

together following synchronization, but not in a linear alignment as for the Abelian case in the example of figure 2, but are spread over a two-dimensional region. Figure 4 shows the trajectory of the unit centre-of-mass vector $\widehat{x}_{\rm CM}(t)$ for $0 \leqslant t \leqslant 120$, for a particular set of initial conditions in which the particle cluster initially circulates the equator with respect to the poles $\pm\widehat{\omega}$, but eventually drifts towards one of the poles. This figure also shows the locations of the individual particles at $t = 120$, evidently bunched together on the surface of the sphere. This picture is confirmed by the values of the parameters $r(t)$ and $d^{(1)}(t)$ plotted in figure 5, which shows that spatial synchronization followed by phase synchronization occurs at about $t = 3.5$. However, since the value of $d^{(1)}(t)$ is asymptotically nonzero, phase locking does not occur, consistent with the fact that (22) is not a limit cycle for any Λ for general frequencies ω_i.

This behaviour, where the particle cluster synchronizes spatially at a fixed latitude and then over time spirals closer to one of the poles, is typical over a range of frequency distributions and initial conditions. It should be mentioned, however, that we have encountered certain frequency distributions for a small number of nodes ($N = 10$), where for all initial conditions the trajectories remain confined to a narrow band at a fixed latitude, which depends on the initial conditions. The width of the band depends on κ, with larger values of κ corresponding to narrower bands.

5.1. The $S^1 \times S^2$ model

We describe here briefly several properties of the 2-sphere model when the $U(1)$ coupling is included, i.e. we consider both sets of equations (17) and (18) in which x_i is a unit 3-vector and Ω_i is given by (28), and where we choose a distribution of frequencies ν_i and ω_i. Trajectories may be analysed and plotted separately on S^1 for the variables θ_i, and on S^2 for the variables x_i. A significant difference compared with the S^2 model is that trajectories, following an initial transient, separate into two disjoint clusters for each of the S^1 and S^2 components, due to negative values acquired by some of the factors $x_i \cdot x_j$ and $\cos(\theta_j - \theta_i)$ which in effect change the sign of κ for couplings between the corresponding nodes i, j. This effect has already been noted in [14] for the Abelian Kuramoto model (1) for the choice $a_{ij} = (-1)^{i-j}$, which leads

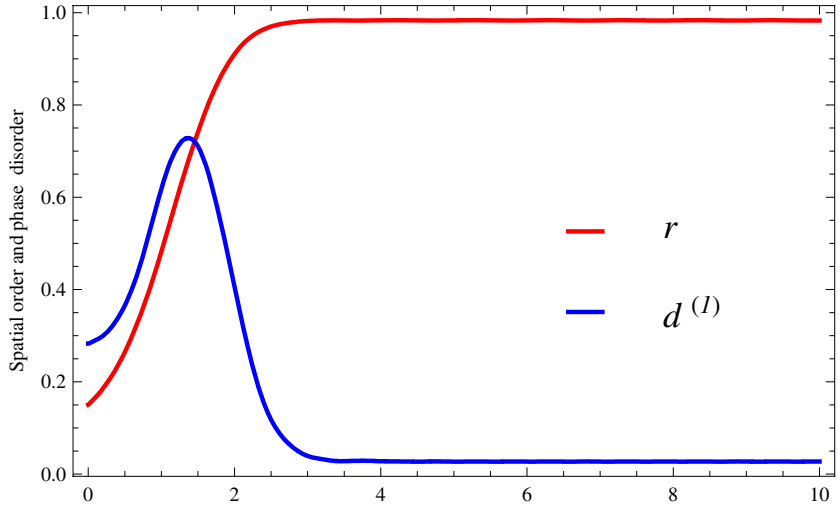

Figure 5. Spatial coherence for the system shown in figure 4 is achieved at $t = 3$ units and for phase coherence at $t = 3.5$ but since $d^{(1)}(t)$ is nonzero for $t > 4$, where $d^{(1)}$ is defined in (23), phase locking does not occur.

to a separation into even and odd nodes. Couplings in this case between either even or odd nodes are unchanged, but even–odd couplings have an effective negative value for κ which leads to a relative displacement of π between even and odd trajectories. Numerical solutions of (17) and (18) for random initial conditions and frequency distributions of ν_i and $\boldsymbol{\omega}_i$ show that neither of the order parameters r, calculated for each of the S^1 and S^2 components, are close to unity, consistent with the observation that trajectories are separated into two disjoint clusters. Phase synchronization however occurs as for the S^2 model, with both S^1 and S^2 trajectories displaying phase coherence, but generally not phase locking, due to the fact that the two particle clusters on S^2 drift to the poles.

It is useful to consider in particular the Abelian case in which $\omega_i^1 = 0 = \omega_i^2$ for which the matrices Ω_i commute for all i, then (17) and (18) may be solved by choosing $x_i^3 = 0$ for all i. If we parametrize $\boldsymbol{x}_i = (\cos\phi_i, \sin\phi_i, 0)$ then (17) and (18) reduce to two sets of equations for the variables θ_i and ϕ_i, which decouple into Abelian Kuramoto equations for the angles $\theta_i^{\pm} = \theta_i \pm \phi_i$. This is evident from the matrix U_i defined in (27), which reduces to

$$U_i = \begin{pmatrix} 0 & \mathrm{i}\,\mathrm{e}^{-\mathrm{i}(\theta_i+\phi_i)} \\ \mathrm{i}\,\mathrm{e}^{-\mathrm{i}(\theta_i-\phi_i)} & 0 \end{pmatrix}.$$

In terms of the original variables θ_i and $\boldsymbol{x}_i$ trajectories on S^1 and S^2 each separate into two clusters, with trajectories on S^2 restricted to the equator, but in terms of the variables $\theta_i^{\pm}$, however, synchronization occurs as for the Abelian Kuramoto model with trajectories restricted to the torus $S^1 \times S^1$. This applies only if the initial positions $\boldsymbol{x}_i(0)$ lie entirely on the equator.

6. The SU(2)×SU(2) model

We now consider the $SU(2) \times SU(2)$ model consisting of equations (2) for $n = 2$ where U_i is parametrized according to (15) with $\theta_i = 0$ for all i, and the 4-vectors $\boldsymbol{x}_i$ satisfy (20) with $m = 4$; trajectories are now confined to S^3. The 4×4 matrices Ω_i are given in terms

of the 3-vector frequencies $\boldsymbol{\omega}_i = (\omega_i^1, \omega_i^2, \omega_i^3)$ by (19), but are not the most general 4×4 antisymmetric matrices in $\mathfrak{so}_4$. Rather, these matrices span an $\mathfrak{su}_2$ subalgebra corresponding to an $SU(2)$ subgroup of the global covariance group $SO(4) \cong SU(2) \times SU(2)$, and the frequency matrix Λ which appears in the limit cycle (22) is an element of the commuting $\mathfrak{su}_2$ subalgebra.

We find that properties of the $SU(2) \times SU(2)$ model resemble those of the Abelian Kuramoto model, in that trajectories are both spatially synchronized and phase-locked with each trajectory tracing out a great circle on S^3, but with the planes of these circles slightly tilted with respect to each other. An exception is the Abelian case, for which all matrices Ω_i commute, when the synchronized trajectories lie in a common two-dimensional plane on S^3, for any initial conditions. The synchronized frequency matrix Λ, as appears in (22), is determined numerically and generally depends on the initial conditions although the synchronized frequency $\lambda = \|\Lambda\|$ depends only on $\boldsymbol{\omega}_i$ and κ.

Natural oscillations at each node are determined by the equations $\dot{\boldsymbol{x}}_i = \Omega_i \boldsymbol{x}_i$, which imply $\ddot{\boldsymbol{x}}_i = \Omega_i^2 \boldsymbol{x}_i$ where Ω_i is given in (19). Since $\Omega_i^2 = -\|\boldsymbol{\omega}_i\|^2 I_4$ all solutions of $\dot{\boldsymbol{x}}_i = \Omega_i \boldsymbol{x}_i$ are given by

$$\boldsymbol{x}_i(t) = \mathrm{e}^{t\Omega_i}\, \boldsymbol{n}_i = \boldsymbol{n}_i \cos(\|\boldsymbol{\omega}_i\| t) + \boldsymbol{m}_i \sin(\|\boldsymbol{\omega}_i\| t), \tag{32}$$

where $\boldsymbol{n}_i, \boldsymbol{m}_i$ are constant orthogonal unit 4-vectors, which are related according to $\boldsymbol{m}_i = \Omega_i \boldsymbol{n}_i / \|\boldsymbol{\omega}_i\|$ and $\boldsymbol{n}_i = -\Omega_i \boldsymbol{m}_i / \|\boldsymbol{\omega}_i\|$. Natural oscillations at the node i are therefore all of the same frequency $\|\boldsymbol{\omega}_i\|$, with trajectories restricted to the two-dimensional plane in $\mathbb{R}^4$ spanned by the vectors $\boldsymbol{m}_i, \boldsymbol{n}_i$. Hence, every such trajectory follows a great circle on S^3.

Limit cycles take the general form (22), that is $\boldsymbol{x}_i(t) = \mathrm{e}^{t\,\Lambda} \boldsymbol{n}_i$ where Λ, an element of $\mathfrak{so}_4$, commutes with Ω_i for every i. The most general form of Λ can be deduced from the non-Abelian limit cycles (8) (where Λ refers to a Hermitean 2×2 matrix), from which we find

$$\Lambda = \begin{pmatrix} 0 & \lambda^3 & -\lambda^2 & -\lambda^1 \\ -\lambda^3 & 0 & \lambda^1 & -\lambda^2 \\ \lambda^2 & -\lambda^1 & 0 & -\lambda^3 \\ \lambda^1 & \lambda^2 & \lambda^3 & 0 \end{pmatrix}, \tag{33}$$

where $\boldsymbol{\lambda} = (\lambda^1, \lambda^2, \lambda^3)$ is a frequency 3-vector. This matrix is evidently antisymmetric and, as may be verified directly, also satisfies $[\Lambda, \Omega_i] = 0$ for all i where Ω_i is given in (19), and is therefore an element of the $\mathfrak{su}_2$ algebra which commutes with Ω_i. We have $\Lambda^2 = -\lambda^2 I_4$ where $\lambda = \|\boldsymbol{\lambda}\| = \|\Lambda\|$, hence the limit cycle has the form

$$\boldsymbol{x}_i(t) = \mathrm{e}^{t\,\Lambda} \boldsymbol{n}_i = \boldsymbol{n}_i \cos \lambda t + \boldsymbol{m}_i \sin \lambda t, \tag{34}$$

where $\boldsymbol{n}_i, \boldsymbol{m}_i$ are constant orthogonal unit 4-vectors with $\boldsymbol{m}_i = \Lambda \boldsymbol{n}_i / \lambda$. Evidently these limit cycles correspond to the natural oscillations (32) but with each natural frequency $\|\boldsymbol{\omega}_i\|$ replaced by the synchronized frequency λ.

We find numerically, for sufficiently large κ with random initial conditions, for natural frequencies $\boldsymbol{\omega}_i = (\omega_i^1, \omega_i^2, \omega_i^3)$ with given random distributions, and with all-to-all coupling, that trajectories are spatially synchronized as measured by the order parameter $r(t)$, which takes a constant value near unity following an initial transient time $t = t_{\mathrm{s}}$. Trajectories are also phase synchronized at time $t = t_{\mathrm{p}} > t_{\mathrm{s}}$ as measured by a zero value for the disorder parameter $d^{(1)}(t)$ defined in (23), for all $t > t_{\mathrm{p}}$. We find that the value of $\boldsymbol{x}_i \cdot \boldsymbol{x}_j$, which is therefore constant in time, is close to unity for each i, j reflecting the fact that the constant distance $\|\boldsymbol{x}_i - \boldsymbol{x}_j\|$ between each pair of particles is small. Since $N^2 r^2 = \sum_{i,j} \boldsymbol{x}_i \cdot \boldsymbol{x}_j$ the constant value of each pair $\boldsymbol{x}_i \cdot \boldsymbol{x}_j$ is approximately r^2. For the limit cycle (34) we have $\|\dot{\boldsymbol{x}}_i(t)\| = \lambda$,

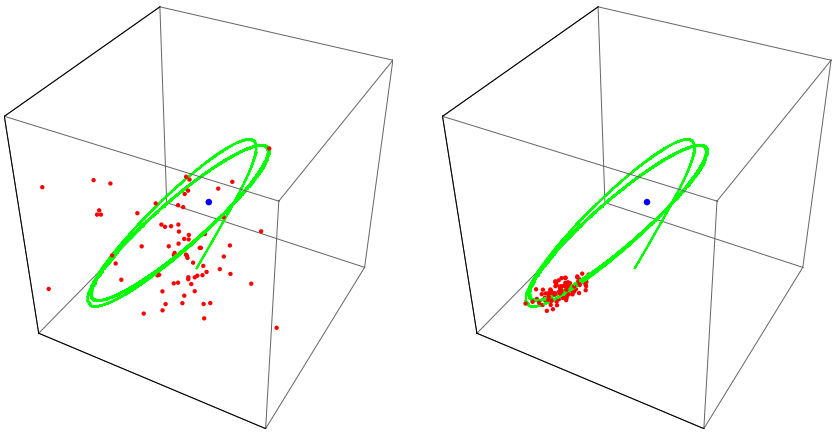

Figure 6. The locations in $\mathbb{R}^3$ of the $N = 100$ particles for $\kappa = 2$, projected stereographically from S^3, showing uncorrelated positions at time $t = 2$ and full synchronization at $t = 6$. The projected unit centre-of-mass trajectory (green), shown for $0 < t < 20$, is a circle following synchronization which lies in a plane through the origin (blue).

independent of i and t, and so we also evaluate the disorder parameter $d^{(2)}(t)$ (following the definition (14)) defined by

$$d^{(2)}(t) = \frac{2}{N(N-1)} \sum_{i<j} \left| \left(\|\dot{\boldsymbol{x}}_i(t)\| - \|\dot{\boldsymbol{x}}_j(t)\| \right) \right| \tag{35}$$

which is also numerically zero for $t > t_{\mathrm{p}}$.

Evaluation of the disorder parameters $d^{(1)}, d^{(2)}$ does not require knowledge of the synchronized frequency matrix Λ which may be found by minimizing $F(\Lambda)$ as defined in (24), with respect to Λ, at any time $t > t_{\mathrm{p}}$. Then we determine that $\sum_i \|\dot{\boldsymbol{x}}_i(t) - \Lambda \boldsymbol{x}_i(t)\|$ is numerically zero for all $t > t_{\mathrm{p}}$. As further confirmation that the numerical solution corresponds to the limit cycle (34), we evaluate $d(t)$ as defined in (25) and find that this parameter is also zero for all $t > t_{\mathrm{p}}$. Hence we establish numerically that synchronized trajectories follow great circles on S^3 which lie in planes that are slightly tilted with respect to each other. An average plane can be defined as that followed by the unit centre of mass $\widehat{\boldsymbol{x}}_{\mathrm{CM}}$, which synchronizes to the limit cycle $\widehat{\boldsymbol{x}}_{\mathrm{CM}}(t) = \mathrm{e}^{t\,\Lambda}\boldsymbol{n}$ where $\boldsymbol{n}$ is a unit 4-vector. The orientation of this plane depends on the initial values $\boldsymbol{x}_i(0)$, as does Λ, however, we find that the synchronized frequency $\lambda = \|\Lambda\|$ depends only on the natural frequencies $\boldsymbol{\omega}_i$ and on κ. In general, for a range of natural frequencies, λ takes a value close but not equal to $\sum_i \|\boldsymbol{\omega}_i\|/N$.

In our numerical calculations we chose Gaussian distributions of standard deviation 0.3 about $\boldsymbol{\omega} = (-2, 1, 2)$ for the frequencies $\boldsymbol{\omega}_i$, with $N = 100$ and $\kappa = 2$, and random initial conditions. Solutions are displayed in figure 6 by means of a stereographic projection, in which 4-vectors $\boldsymbol{x}_i$ on S^3 are mapped to 3-vectors $\boldsymbol{u}_i$ in $\mathbb{R}^3$ according to

$$\boldsymbol{u}_i = \frac{(x_i^1, x_i^2, x_i^3)}{1 - x_i^4}.$$

The particle locations are shown at time $t = 2$ units, spatially uncorrelated, and also at $t = 6$ fully synchronized, together with the projected unit centre-of-mass $\widehat{\boldsymbol{x}}_{\mathrm{CM}}(t)$ trajectory, which is a circle lying in a plane through the origin. Figure 7 shows firstly the order parameter $r(t)$ as a function of time, revealing that spatial synchronization occurs at $t = 4$ units, and secondly the disorder parameter $d(t)$ defined in (25), which is apparently zero for $t \geqslant 5$ but in fact

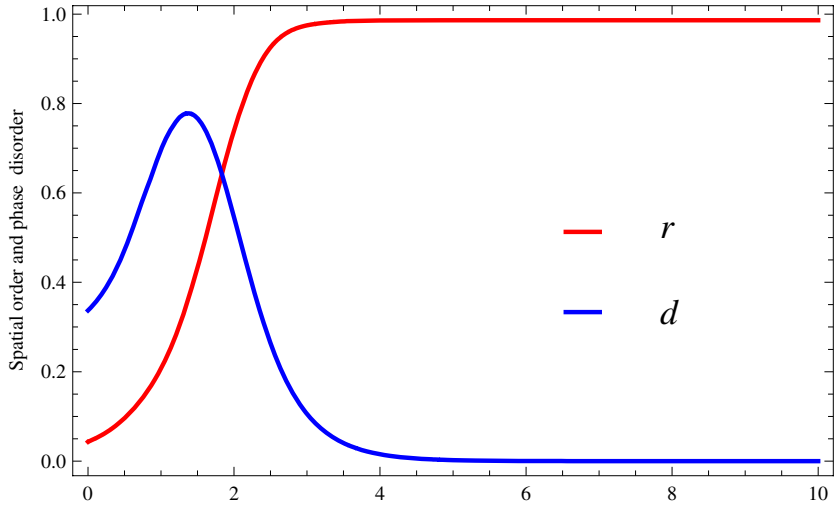

Figure 7. Spatial coherence for the system shown in figure 6 is achieved at $t = 4$ and phase locking occurs at $t = 5$ when $d(t)$ is zero, where d is defined in (25).

decreases monotonically from $t = 2$ until such time $t > 8$ when numerical error becomes significant. Disorder parameters such as $d^{(2)}(t)$ defined in (35) and others discussed above are also numerically zero following phase synchronization. Hence all trajectories become phase-locked and are numerically indistinguishable from the limit cycles (34).

For the Abelian case, for which the matrices Ω_i in (19) commute for all i, synchronization occurs with properties similar to those for the general case. In particular if we choose $\omega_i^1 = 0 = \omega_i^2$ for all i and set either $x_i^3 = 0 = x_i^4$ or $x_i^1 = 0 = x_i^2$ then (20) reduces to the Abelian Kuramoto model. Hence, if the particles initially lie in the X^3–X^4 plane, or the X^1–X^2 plane, then subsequent trajectories also lie in the same plane and synchronization takes place as for the Abelian Kuramoto model. If we choose random initial positions on S^3 with $\omega_i^1 = 0 = \omega_i^2$ for all i, then we find that synchronization with phase locking occurs in which all synchronized trajectories lie on a common great circle on S^3, which therefore coincides with the trajectory of the unit centre of mass. This means that all particles are aligned linearly on a common circle, as for the Abelian Kuramoto model, however the plane in which this circle lies depends on the initial conditions since, as already discussed, trajectories initially in either the X^1–X^2 plane or X^3–X^4 plane remain within that plane. This is consistent with the previous observation that the synchronization matrix Λ depends on the initial conditions, however we do find in this case that the synchronized frequency $\|\Lambda\|$ is equal to the average natural frequency $\sum_i \|\omega_i\|/N$, and so is also independent of κ. In general, therefore, we find for the case of Abelian matrices Ω_i that synchronized trajectories behave like those of the Abelian Kuramoto model and are restricted to a common unit circle on S^3, the orientation of which depends on the frequencies ω_i, the initial values $x_i(0)$, and on κ.

6.1. The SO(3)×SO(3) model

We discuss here briefly the model consisting of equations (5) for $n = 3$ where the 3×3 matrices $J_i = 2\Omega_i$ are elements of $\mathfrak{so}_3$ with Ω_i given in (28). As one would expect, this model is related to the $SU(2) \times SU(2)$ model discussed in the previous section, as follows by parametrizing an $SO(3)$ matrix O in terms of a corresponding $SU(2)$ matrix U according to

$(O)_{rs} = \frac{1}{2}\mathrm{Tr}(\sigma_r U \sigma_s U^\dagger)$, which defines a homomorphism that maps elements $\pm U$ of $SU(2)$ to $O \in SO(3)$. We may parametrize each U_i by means of a unit 4-vector $\boldsymbol{x}_i$ according to (15), setting $\theta_i = 0$, and hence parametrize elements of $SO(3)$ in terms of unit 4-vectors $\boldsymbol{x}_i$. Specifically, if we write $\boldsymbol{x} = (x, y, z, w)$ with $x^2 + y^2 + z^2 + w^2 = 1$ then

$$O = \begin{pmatrix} x^2 - y^2 - z^2 + w^2 & 2(xy + zw) & 2(xz - yw) \\ 2(xy - zw) & -x^2 + y^2 - z^2 + w^2 & 2(xw + yz) \\ 2(xz + yw) & 2(yz - xw) & -x^2 - y^2 + z^2 + w^2 \end{pmatrix}$$

is an element of $SO(3)$. With this parametrization equations (5) reduce to

$$\|\boldsymbol{x}_i\|^4 \dot{\boldsymbol{x}}_i = \Omega_i \boldsymbol{x}_i + \frac{\kappa}{N} \sum_{j=1}^{N} a_{ij} \boldsymbol{x}_i \cdot \boldsymbol{x}_j \left(\|\boldsymbol{x}_i\|^2 \boldsymbol{x}_j - \boldsymbol{x}_i \cdot \boldsymbol{x}_j \boldsymbol{x}_i \right), \tag{36}$$

for $i = 1, \ldots, N$ where $\boldsymbol{x}_i$ is a 4-vector and Ω_i is the 4×4 matrix given by (19). As before, these equations imply $\boldsymbol{x}_i \cdot \dot{\boldsymbol{x}}_i = 0$ and hence we may set $\|\boldsymbol{x}_i\| = 1$ in (36), however these equations differ from (20) in that a_{ij} is replaced by $a_{ij}\, \boldsymbol{x}_i \cdot \boldsymbol{x}_j$. Unlike (20), the $4N$ equations (36) are invariant under the replacement $\boldsymbol{x}_i \to -\boldsymbol{x}_i$ for any fixed i, with $\boldsymbol{x}_j$ unchanged for all other values $j \neq i$. This is a consequence of the two-to-one mapping from $SU(2)$ to $SO(3)$.

Phase-locked synchronization occurs as for the $SU(2) \times SU(2)$ model for sufficiently large κ, in particular, when synchronized, all pairs $|\boldsymbol{x}_i \cdot \boldsymbol{x}_j|$ are constant in time with a value close to unity, which means that synchronization occurs with a slightly reduced effective value for κ. However because $\boldsymbol{x}_i \cdot \boldsymbol{x}_j$ can also take constant negative values for some pairs i, j, the coupling κ between such pairs is effectively negative, which separates the cluster of N particles into two disjoint groups in a way similar to that described in section 5.1. Consistent with this, we find numerically that even when phase locking has occurred the order parameter r takes a constant value which is significantly less than unity, following the initial transient. The existence of phase locking can be verified by calculating the various phase disorder measures previously discussed, for example one may calculate Λ by minimizing $F(\Lambda)$ as in (24), and then evaluate $d(t)$ in (25), which we find approaches zero following the initial transient.

7. Spatial synchronization and fixed points

We discuss here firstly spatial synchronization in the S^{m-1} models, restricted to all-to-all coupling, and provide at least a partial explanation as to why particles tend to bunch together for sufficiently large κ, independent of whether the motion is phase synchronized, assuming that some clustering has already occurred. We then investigate fixed point solutions, a topic which together with a stability analysis has been extensively studied for the Abelian Kuramoto model, see for example [21–23], where our aim is to identify general properties of the fixed points without proving stability. We write equations (20) of the S^{m-1} model in the form

$$\dot{\boldsymbol{x}}_i = \Omega_i \boldsymbol{x}_i + \kappa \boldsymbol{x}_{\mathrm{CM}} - \kappa \boldsymbol{x}_i \, (\boldsymbol{x}_i \cdot \boldsymbol{x}_{\mathrm{CM}}) \qquad (i = 1, \ldots, N), \tag{37}$$

where $\boldsymbol{x}_i$ is a unit m-vector at the node i, $\boldsymbol{x}_{\mathrm{CM}}$ is defined by (21) and $\kappa > 0$. Each node couples to other nodes through $\boldsymbol{x}_{\mathrm{CM}}$, as for the Abelian case.

7.1. Qualitative properties of spatial synchronization

Spatial synchronization, in which r takes a constant value near unity, occurs for the S^{m-1} models (although not for the models discussed in sections 5.1 and 6.1) even though phase locking does not necessarily occur, as in the S^2 model. In order for spatial synchronization to occur for random initial conditions the distance $\|\boldsymbol{x}_i - \boldsymbol{x}_j\|$ between any two particles i, j must

decrease with time, although not necessarily monotonically. We evaluate this rate of change by calculating $\dot{\boldsymbol{x}}_i \cdot \boldsymbol{x}_j + \boldsymbol{x}_i \cdot \dot{\boldsymbol{x}}_j$ from (37) and hence determine that

$$\frac{\mathrm{d}}{\mathrm{d}t}\|\boldsymbol{x}_i - \boldsymbol{x}_j\| = \widehat{\boldsymbol{x}}_{i-j} \cdot (\Omega_i \boldsymbol{x}_i - \Omega_j \boldsymbol{x}_j) - \kappa \|\boldsymbol{x}_i - \boldsymbol{x}_j\|(\boldsymbol{x}_{i+j} \cdot \boldsymbol{x}_{\mathrm{CM}}), \tag{38}$$

where $\widehat{\boldsymbol{x}}_{i-j} = (\boldsymbol{x}_i - \boldsymbol{x}_j)/\|\boldsymbol{x}_i - \boldsymbol{x}_j\|$ and $\boldsymbol{x}_{i+j} = (\boldsymbol{x}_i + \boldsymbol{x}_j)/2$. The magnitude of the first term on the right-hand side is bounded above by $\|\Omega_i\| + \|\Omega_j\|$, whereas the last term is bounded by $\kappa\, r\, \|\boldsymbol{x}_i - \boldsymbol{x}_j\| \leqslant 2\kappa$ where $r = \|\boldsymbol{x}_{\mathrm{CM}}\|$. For sufficiently large κ the last term is dominant and provided the inner product $(\boldsymbol{x}_{i+j} \cdot \boldsymbol{x}_{\mathrm{CM}})$ is bounded below by a positive number for all i, j, as occurs for example if all particles are located in a common hemisphere of S^{m-1}, then the right-hand side of (38) is negative. Then $\|\boldsymbol{x}_i - \boldsymbol{x}_j\|$ decreases monotonically with time while $(\boldsymbol{x}_{i+j} \cdot \boldsymbol{x}_{\mathrm{CM}})$ remains positive, i.e. particles bunch further together and so synchronize spatially. This is indicated by a value of r near unity, as follows from $2N^2(1 - r^2) = \sum_{i,j} \|\boldsymbol{x}_i - \boldsymbol{x}_j\|^2$, which demonstrates that $r \approx 1$ corresponds to a small value for each distance $\|\boldsymbol{x}_i - \boldsymbol{x}_j\|$.

As $\boldsymbol{x}_i$ approaches $\boldsymbol{x}_j$ the effective coupling $\kappa\, r\, \|\boldsymbol{x}_i - \boldsymbol{x}_j\|$ in (38) eventually reduces for any fixed κ to a value comparable to $\|\Omega_i\| + \|\Omega_j\|$, and the right-hand side of (38) then becomes indefinite in sign. The particle cluster becomes more tightly bunched therefore only if κ is increased. Similarly, if two nodes i, j are co-located, i.e. $\boldsymbol{x}_i = \boldsymbol{x}_j$ initially, then the time derivative of $\|\boldsymbol{x}_i - \boldsymbol{x}_j\|$ is nonzero and so the particles i, j separate. If there exist one or more nodes i for which $\|\Omega_i\|$ is larger than fixed 2κ, the right-hand side of (38) is of indefinite sign, and such nodes i therefore do not spatially synchronize with other nodes j. These considerations are independent of whether phase locking occurs.

7.2. Fixed points

Consider now fixed point solutions to equations (37), but omitting the question of stability of such solutions. Keeping in mind the limit cycle (22) we define the unit vectors $\boldsymbol{n}_i(t) = \mathrm{e}^{-t\,\Lambda}\boldsymbol{x}_i(t)$, where we assume that there exists a real $m \times m$ matrix Λ which is antisymmetric and commutes with Ω_i for all i, but is for now otherwise unspecified. We denote by $\boldsymbol{n}_{\mathrm{CM}} = \mathrm{e}^{-t\,\Lambda}\widehat{\boldsymbol{x}}_{\mathrm{CM}}$ the rotated unit centre-of-mass vector which is also defined by $\boldsymbol{n}_{\mathrm{CM}} = \sum_i \boldsymbol{n}_i/(Nr)$ where $r = \|\boldsymbol{x}_{\mathrm{CM}}\|$. Then (37) is equivalent to

$$\dot{\boldsymbol{n}}_i = (\Omega_i - \Lambda)\boldsymbol{n}_i + \kappa r \boldsymbol{n}_{\mathrm{CM}} - \kappa r \boldsymbol{n}_i(\boldsymbol{n}_i \cdot \boldsymbol{n}_{\mathrm{CM}}).$$

We look for fixed point solutions of these equations and hence, setting $\dot{\boldsymbol{n}}_i = 0$, we have

$$(\Omega_i - \Lambda)\boldsymbol{n}_i = \kappa\, r\, \boldsymbol{n}_i\, (\boldsymbol{n}_i \cdot \boldsymbol{n}_{\mathrm{CM}}) - \kappa\, r\, \boldsymbol{n}_{\mathrm{CM}}. \tag{39}$$

Squaring both sides gives

$$\|(\Omega_i - \Lambda)\boldsymbol{n}_i\|^2 = \kappa^2 r^2 \left[1 - (\boldsymbol{n}_i \cdot \boldsymbol{n}_{\mathrm{CM}})^2\right]. \tag{40}$$

It follows that $\|(\Omega_i - \Lambda)\boldsymbol{n}_i\| \leqslant \kappa\, r$ and hence $\|(\Omega_i - \Lambda)\boldsymbol{n}_i\| \leqslant \kappa$ at each node i, in order that a fixed point solution should exist. Since $|(\|\Omega_i \boldsymbol{n}_i\| - \|\Lambda \boldsymbol{n}_i\|)| \leqslant \|(\Omega_i - \Lambda)\boldsymbol{n}_i\|$ we see, consistent with (10), that the natural frequencies should be close to the synchronized frequencies for fixed point solutions $\boldsymbol{n}_i$ to exist.

The fact that the inequalities $\|(\Omega_i - \Lambda)\boldsymbol{n}_i\| \leqslant \kappa$ must be satisfied for all i suggests, as discussed in section 3, that we define Λ as the matrix that minimizes the function

$$F(\Lambda) = \frac{1}{N}\sum_{i=1}^{N} \|(\Omega_i - \Lambda)\boldsymbol{n}_i\|^2\,. \tag{41}$$

Although we do not prove that fixed points with this property are stable, we may verify that Λ minimizes F for known cases. For $m = 2$ we have $\Omega_i = \nu_i\, \imath_2$, $\Lambda = \lambda\, \imath_2$ where $\imath_2$ is

given in (6), hence $\|(\Omega_i - \Lambda)\boldsymbol{n}_i\|^2 = (\nu_i - \lambda)^2$ and therefore $F(\lambda)$ is minimized correctly by $\lambda = \sum_i \nu_i/N$.

For $m = 4$ the matrices Ω_i, Λ, which commute for all i, are given by (19), (33) respectively and satisfy $\Omega_i^2 = -\|\boldsymbol{\omega}_i\|^2 I_4$ where $\boldsymbol{\omega}_i = (\omega_i^1, \omega_i^2, \omega_i^3)$, and $\Lambda^2 = -\lambda^2 I_4$ where $\lambda = \|\Lambda\| = \|\boldsymbol{\lambda}\|$, with $\boldsymbol{\lambda} = (\lambda^1, \lambda^2, \lambda^3)$. As shown in the limit cycle (34), λ is the synchronization frequency. We may write $\Lambda = \sum_{\alpha=1}^3 \lambda_\alpha K_\alpha$ where the $\mathfrak{so}_3$ generators (K_1, K_2, K_3) can be identified from (33), and satisfy the Pauli algebra $\{K_\alpha, K_\beta\} = -2\delta_{\alpha\beta} I_4$. The function F defined by (41) is given by

$$F(\lambda_1, \lambda_2, \lambda_3) = \lambda^2 + \frac{1}{N}\sum_{i=1}^N \|\boldsymbol{\omega}_i\|^2 + \frac{2}{N}\sum_{\alpha=1}^3 \sum_{i=1}^N \lambda_\alpha (\boldsymbol{n}_i \cdot K_\alpha \Omega_i \boldsymbol{n}_i),$$

and the minimum occurs at

$$\lambda_\alpha = -\frac{1}{N}\sum_{i=1}^N (\boldsymbol{n}_i \cdot K_\alpha \Omega_i \, \boldsymbol{n}_i), \qquad \alpha = 1, 2, 3. \tag{42}$$

The frequency λ is determined from this formula and also satisfies as a consequence

$$\lambda^2 = -\frac{1}{N}\sum_{i=1}^N (\boldsymbol{n}_i \cdot \Lambda \Omega_i \, \boldsymbol{n}_i). \tag{43}$$

This particular equation can also be derived from (39) by premultiplying by Λ, taking the inner product with $\boldsymbol{n}_i$, and summing over i. Since $\|\Omega_i\| = \|\boldsymbol{\omega}_i\|$, it follows that $\lambda \leqslant \sum_i \|\boldsymbol{\omega}_i\|/N$, independent of the initial conditions and also κ.

Numerical computations, as discussed in section 6, agree with these formulas. For any given numerical solution $\boldsymbol{x}_i(t)$ it is convenient to determine Λ by minimizing $F(\Lambda)$ as given in (24) with respect to Λ, at any fixed time following synchronization. We find that the fixed points $\boldsymbol{n}_i$, the vector $\boldsymbol{n}_{\text{CM}}$, and the matrix Λ all depend on the initial values $\boldsymbol{x}_i(0)$ as well as on the natural frequencies $\boldsymbol{\omega}_i$ and on κ. As found in section 6, the orientation of each two-dimensional plane of a synchronized trajectory on S^3 depends on the initial conditions. We find numerically, however, that the frequencies ρ_i defined by

$$\rho_i = \|(\Omega_i - \Lambda)\boldsymbol{n}_i\| = \|(\Omega_i - \Lambda)\boldsymbol{x}_i\| \tag{44}$$

are independent of $\boldsymbol{x}_i(0)$, i.e. each ρ_i depends only on the natural frequencies $\boldsymbol{\omega}_1, \ldots, \boldsymbol{\omega}_N$ and on κ. Hence from (40), and confirmed also numerically, $\boldsymbol{n}_i \cdot \boldsymbol{n}_{\text{CM}}$ is independent of $\boldsymbol{x}_i(0)$, as is the synchronized frequency λ, the scalars $2\boldsymbol{n}_i \cdot \Lambda\Omega_i\boldsymbol{n}_i = \rho_i^2 - \|\boldsymbol{\omega}_i\|^2 - \lambda^2$, and the minimum of F, which takes the value

$$F_{\min} = \frac{1}{N}\sum_{i=1}^N \rho_i^2 = -\lambda^2 + \frac{1}{N}\sum_{i=1}^N \|\boldsymbol{\omega}_i\|^2,$$

even though the location of the minimum depends on $\boldsymbol{x}_i(0)$.

The inequality $\lambda \leqslant \sum_i \|\boldsymbol{\omega}_i\|/N$ is also satisfied numerically, with equality for the Abelian case in which the matrices Ω_i mutually commute for all i. Evidently in this case the unit 3-vectors $\boldsymbol{v}_i = (v_i^1, v_i^2, v_i^3)$, where

$$v_i^\alpha = \frac{1}{\|\boldsymbol{\omega}_i\|}\boldsymbol{n}_i \cdot K_\alpha \Omega_i \boldsymbol{n}_i,$$

are parallel and therefore independent of i. We may set $\boldsymbol{v}_i = \boldsymbol{v}$ for each i, and so for the Abelian case we have

$$\boldsymbol{\lambda} = -\frac{\boldsymbol{v}}{N}\sum_{i=1}^{N}\|\boldsymbol{\omega}_i\|.$$

We also find, as for $m = 2$, that λ is independent of κ. For general Ω_i, however, the unit vectors $\boldsymbol{v}_i$ are not quite parallel and we have the formula, from (42), $\boldsymbol{\lambda} = -\sum_i(\|\boldsymbol{\omega}_i\|\boldsymbol{v}_i)/N$. The synchronized frequency λ now depends on κ as well as the natural frequencies $\boldsymbol{\omega}_i$.

Returning now to (40) for general m, with the definition (44) we have

$$\boldsymbol{n}_i \cdot \boldsymbol{n}_{\rm CM} = \sqrt{1 - \frac{\rho_i^2}{\kappa^2 r^2}}, \tag{45}$$

where we assume that only positive signs are permitted in taking the square root. This is proved for the Abelian case $m = 2$ in [21], also [23], and numerically we find $\boldsymbol{n}_i \cdot \boldsymbol{n}_{\rm CM} > 0$ to be valid also for $m = 4$ in section 6. Generally, from the equation $2N(1-r) = \sum_i \|\boldsymbol{n}_i - \boldsymbol{n}_{\rm CM}\|^2$ we have the inequality $\|\boldsymbol{n}_i - \boldsymbol{n}_{\rm CM}\|^2 \leqslant 2N(1-r)$ for each i, which implies $\boldsymbol{n}_i \cdot \boldsymbol{n}_{\rm CM} \geqslant 1 - N(1-r)$ and so provided $1 - r \leqslant 1/N$, which holds for sufficiently large κ, we have $\boldsymbol{n}_i \cdot \boldsymbol{n}_{\rm CM} \geqslant 0$ for all i. The $SO(3) \times SO(3)$ model described in section 6.1 violates these inequalities, however, since phase locking occurs without spatial synchronization.

The sum $\sum_i \boldsymbol{n}_i \cdot \boldsymbol{n}_{\rm CM} = N r$ implies

$$\frac{1}{N}\sum_{i=1}^{N}\sqrt{1 - \frac{\rho_i^2}{\kappa^2 r^2}} = r \tag{46}$$

which, for fixed frequencies ρ_i, determines r as a function of κ. Solutions exist only for $\kappa \geqslant \max_i \rho_i$. We follow the analysis of Mirollo and Strogatz [21] (section 3 on locked states) by defining

$$f(x) = \frac{1}{N}\sum_{i=1}^{N}\sqrt{x - \rho_i^2},$$

where $x = \kappa^2 r^2$, and look for solutions of $\kappa f(x) = x$. The domain of f is $[\rho^2, \infty)$ where $\rho = \max_i \rho_i$ and f satisfies various properties as described in [21]. There exist two critical values of κ, $\kappa_{\rm c} < \kappa_{\rm c}'$ such that

(a) for $0 < \kappa < \kappa_{\rm c}$ there are no solutions to $\kappa f(x) = x$;
(b) for $\kappa = \kappa_{\rm c}$ there is one solution to $\kappa f(x) = x$;
(c) for $\kappa_{\rm c} < \kappa \leqslant \kappa_{\rm c}'$ there are two solutions to $\kappa f(x) = x$;
(d) for $\kappa_{\rm c}' < \kappa$ there is one solution to $\kappa f(x) = x$.

Any $x \in [\rho^2, \infty)$ determines a solution (r, κ) to (46) with $r = f(x)/\sqrt{x}$ and $\kappa = x/f(x)$. There is a unique critical value $x_{\rm c}$ such that $f'(x_{\rm c}) = f(x_{\rm c})/x_{\rm c}$, and so any $x \in (x_{\rm c}, \infty)$ parametrizes a solution (r, κ) to (46) with

$$r > r_{\rm c} = \frac{f(x_{\rm c})}{\sqrt{x_{\rm c}}}, \qquad \kappa > \kappa_{\rm c} = \frac{x_{\rm c}}{f(x_{\rm c})}.$$

It is shown in [21] that for $m = 2$ all such solutions lead to stable fixed points.

In summary, given the matrices Ω_i of natural frequencies and a coupling constant κ, we find the fixed points $\boldsymbol{n}_i$ in principle by firstly evaluating the frequencies $\rho_1, \ldots, \rho_N$ which are functions only of Ω_i and κ (although we have no closed formula for these functions), and then determining a solution $r = r(\kappa)$ to (46). Then from (45) we find the scalars $\boldsymbol{n}_i \cdot \boldsymbol{n}_{\rm CM}$. We now

solve equations (39), which we regard as a set of linear equations for the N unit m-vectors $\boldsymbol{n}_1, \ldots, \boldsymbol{n}_N$ (recalling that $r\,\boldsymbol{n}_{\rm CM} = \sum_i \boldsymbol{n}_i/N$), while simultaneously minimizing F in (41) in order to find Λ. The solution is not unique, since for any fixed point $\boldsymbol{n}_i$ another solution is $e^{t_0\,\Lambda}\boldsymbol{n}_i(t)$, where t_0 is any parameter. The Abelian case $m = 2$ is of course much simpler because $\Lambda = \lambda\,\imath_2$ is known explicitly, as is $\rho_i^2 = (\nu_i - \lambda)^2$, and so (39) may be solved directly.

As a final remark, for $m = 2$ it is known [24] that the defining equations can be expressed in the gradient form $\dot\theta = -\nabla_\theta \Phi$, where $\theta = (\theta_i)$ denotes the N-vector of all components, for a scalar function Φ. This property is useful for a stability analysis [24, 21] but can be only partially generalized to equations (17), (18), where $\boldsymbol{x}_i$ denotes m-vectors. Taking now a general connectivity matrix (a_{ij}), we define the scalar functions

$$\Phi_i(\theta_1, \ldots, \theta_N, \boldsymbol{x}_1, \ldots, \boldsymbol{x}_N) = -\sum_{j=1}^N \nu_j\theta_j - \frac{\kappa}{N}\sum_{j=1}^N a_{ij}\cos(\theta_j - \theta_i)\frac{\boldsymbol{x}_i}{\|\boldsymbol{x}_i\|}\cdot\frac{\boldsymbol{x}_j}{\|\boldsymbol{x}_j\|},$$

for $i = 1, \ldots, N$. Each Φ_i is defined on the N-torus T^N with respect to the variables θ_i, and on $\mathbb{R}^{mN}\backslash\{0\}$ with respect to the N unconstrained m-vectors $\boldsymbol{x}_i$. Equations (17) and (18) may be written in the equivalent form

$$\dot\theta_i = -\frac{\partial\Phi_i}{\partial\theta_i}, \qquad \dot{\boldsymbol{x}}_i = \Omega_i\boldsymbol{x}_i - \nabla_i\Phi_i,$$

where ∇_i refers to the gradient with respect to $\boldsymbol{x}_i$; however, for $m > 2$ the term $\Omega_i\boldsymbol{x}_i$ cannot conveniently be expressed as the gradient of a scalar function.

8. Conclusion

We have defined essentially two generalizations of the Kuramoto model and identified the main features of each. The first generalization consists of the chirally covariant models (2) which can be formulated for any classical compact Lie group and have properties similar to the Abelian Kuramoto model, such as synchronization of trajectories with phase locking for coupling strengths greater than some critical value. Limit cycles exist for all such models and we have investigated numerical solutions for the $SU(2) \times SU(2)$ case. Synchronization frequencies are determined by minimizing a quadratic function of the trajectories, but do not generally have a simple expression in terms of the natural frequencies.

The second generalization consists of models such as (26) with a broken chiral symmetry, which we have formulated as S^{m-1} models and for which phase synchronization and limit cycles exist only under special conditions. Numerical results for $m = 3$ indicate that although spatial synchronization generally occurs, phase coherence is not exact and that trajectories are attracted towards a fixed point.

These non-Abelian models provide a means of synchronizing processes with many degrees of freedom at each node. There remain, of course, many aspects of synchronization still to be investigated, such as partial synchronization for weak couplings, the effect of nontrivial network connections with a large number of nodes, specific properties of the models for higher rank symmetry groups, as well as a classification and proof of stability of all fixed points, special properties as $N \to \infty$, and topological properties.

Acknowledgment

I gratefully acknowledge the support of the Larry Biedenharn Fellowship.

References

[1] Strogatz S 2001 *Nature* **410** 268–76
[2] Strogatz S 2003 *SYNC: The Emerging Science of Spontaneous Order* (New York: Hyperion Books)
[3] Pikovsky A, Rosenblum M and Kurths J 2001 *Synchronization* (Cambridge: Cambridge University Press)
[4] Osipov G V, Kurths J and Zhou C 2007 *Synchronization in Oscillatory Networks* (Berlin: Springer)
[5] Strogatz S 2000 *Physica* D **143** 1–20
[6] Boccaletti S, Kurths J, Osipov G, Valladares D L and Zhou C S 2002 *Phys. Rep.* **366** 1–101
[7] Acebrón J A, Bonilla L L, Pérez-Vicente C J, Ritort F and Spigler R 2005 *Rev. Mod. Phys.* **77** 137–85
[8] Boccaletti S, Latora V, Moreno Y, Chavez M and Hwang D-U 2006 *Phys. Rep.* **424** 175–308
[9] Arenas A, Díaz-Guilera A, Kurths J, Moreno Y and Zhou C 2008 *Phys. Rep.* **469** 93–153
[10] Strogatz S H 2003 Obituaries: Arthur T Winfree *SIAM News* January **36**
[11] Winfree A T 1980 *The Geometry of Biological Time* (Berlin: Springer)
[12] Kuramoto Y 1975 in *International Symposium on Mathematical Problems in Theoretical Physics* (*Lect. Notes Phys.* vol 39) ed ed H Araki, pp 420–2
[13] Kuramoto Y 1984 *Chemical Oscillations, Waves, and Turbulence* (New York: Springer)
[14] Platten S, Moran P and Lohe M A Measures of synchronization (in preparation)
[15] Horn R A and Johnson C R 1991 *Matrix Analysis* (New York: Cambridge)
[16] Sakaguchi H 1988 *Prog. Theor. Phys.* **79** 39–46
[17] Ott E and Antonsen T M 2008 *Chaos* **18** 037113
[18] Gu Z-M, Zhao M, Zhou T, Zhu C-P and Wang B-H 2007 *Phys. Lett.* A **362** 115–9
[19] Isaacson E and Keller H B 1966 *Analysis of Numerical Methods* (New York: Wiley)
[20] Ritort F 1998 *Phys. Rev. Lett.* **80** 6–9
[21] Mirollo R E and Strogatz S H 2005 *Physica* D **205** 249–66
[22] Mirollo R and Strogatz S H 2007 *J. Nonlinear Sci.* **17** 309–47
Mirollo R and Strogatz S H 2007 *J. Nonlinear Sci.* **18** 219–20
[23] Aeyels D and Rogge J A 2004 *Prog. Theor. Phys.* **112** 921–42
[24] van Hemmen J L and Wreszinski W F 1993 *J. Stat. Phys.* **72** 145–66